

Ensemble dependence of Critical Casimir Forces in Films with Dirichlet Boundary Conditions

Christian M. Rohwer,^{1,2,*} Alessio Squarcini,^{1,2} Oleg Vasilyev,^{1,2} S. Dietrich,^{1,2} and Markus Gross^{1,2,†}

¹Max Planck Institute for Intelligent Systems, Heisenbergstr. 3, 70569 Stuttgart, Germany

²4th Institute for Theoretical Physics, Universität Stuttgart, Pfaffenwaldring 57, 70569 Stuttgart, Germany

(Dated: September 16, 2021)

In a recent study [Phys. Rev. E **94**, 022103 (2016)] it has been shown that, for a fluid film subject to critical adsorption, the resulting critical Casimir force (CCF) may significantly depend on the thermodynamic ensemble. Here, we extend that study by considering fluid films within the so-called ordinary surface universality class. We focus on mean-field theory, within which the order parameter (OP) profile satisfies Dirichlet boundary conditions and produces a nontrivial CCF in the presence of external bulk fields or, respectively, a nonzero total order parameter within the film. Additionally, we study the influence of fluctuations by means of Monte Carlo simulations of the three-dimensional Ising model. We show that, in the canonical ensemble, i.e., when fixing the so-called total mass within the film, the CCF is repulsive for large absolute values of the total OP, instead of attractive as in the grand canonical ensemble. Based on the Landau-Ginzburg free energy, we furthermore obtain analytic expressions for the order parameter profiles and analyze the relation between the total mass in the film and the external bulk field.

I. INTRODUCTION

Confining a critical fluid by parallel walls gives rise to a critical Casimir force (CCF) acting on the bounding surfaces [1, 2]. Here we consider fluids belonging to the Ising bulk universality class (UC), which, accordingly, are described by a one-component order parameter (OP) field ϕ . The bulk UC splits up into several surface UCs, describing further universal properties induced by the surfaces [3–5]. In a classical fluid, the constituent molecules are generically attracted towards an immersed solid surface. This attraction can be either strong or weak compared with the liquid-liquid interaction. Accordingly, for a one-component fluid the surfaces have a preference either for its liquid phase (in the case of a strong substrate) or the vapor phase (in the case of a weak substrate), whereas for a binary liquid mixture the walls attract that phase which is rich in the species preferred by the surfaces. Near the critical point, this attraction gives rise to the phenomenon of critical adsorption, which, in the limit of infinitely strong adsorption (surface field $h_1 \rightarrow \infty$), is described by the so-called *normal* surface UC [6–8]. Fluids show also an enhanced molecular order near a solid surface [3, 8], which is modeled field-theoretically by a so-called surface enhancement parameter c . The limit $c \rightarrow \infty$ (for finite adsorption strength h_1) defines the so-called *ordinary* surface UC, in which the OP effectively satisfies Dirichlet boundary conditions.

While critical fluids are typically strongly adsorbed at

container walls [9], by suitable preparation of the surfaces it is nevertheless possible to approach the limit of weak adsorption, corresponding to the ordinary surface UC. In Ref. [10], this has been achieved by chemical treatment of the surface, while in Refs. [11–14] surface patterning has been used.

The CCF stems from residual finite-size contributions of the free energy of the film. Remarkably, as has been shown in Refs. [15, 16], the amplitude and the scaling function of the CCF depend not only on the bulk and the surface UC, but also on the thermodynamic ensemble under consideration. In fact, CCFs are typically studied for fluid films which can exchange particles with their environment—a situation which realizes the grand canonical ensemble. However, global OP conservation, which is applicable for the canonical ensemble, can induce drastic changes of the CCF [15, 16]. Hitherto, only a few studies have focused on the effect of a global OP constraint on the critical behavior [17–21]. In the present study, building on Ref. [15] (where critical adsorption has been investigated), we consider Ising-type fluid films within the ordinary surface UC, subject to a global OP constraint. We focus on mean-field theory, within which the effects of fluctuations are neglected and the CCF is a consequence of the presence of a spatially varying OP profile across the film.

In the grand canonical ensemble, a nonzero external bulk field μ acting in the film does induce a nontrivial OP profile. In the canonical ensemble, instead, a nonzero value Φ of the total integrated OP, henceforth called the *mass*, is imposed:

$$\Phi \equiv A \int_0^L dz \phi(z). \quad (1)$$

* crohwer@is.mpg.de

† gross@is.mpg.de

Here A denotes the transverse area of the film, L its thickness, and z the associated transverse coordinate. We generally assume the film to be homogeneous in the remaining, lateral directions. Henceforth we consider all extensive quantities, such as Φ , as quantities *per transverse area* A , i.e., $\int_0^L dz \phi(z)$. We find that the OP constraint in Eq. (1) can change, *inter alia*, the character of the CCF from attractive in the grand canonical case to repulsive in the canonical case.

In passing, we recall that, for a critical fluid film within the ordinary surface UC, the critical temperature T_c is shifted from its bulk value T_c^b to $T_c^f < T_c^b$. For Dirichlet boundary conditions and vanishing external fields $\mu = 0$, the OP profile vanishes above the film critical point, i.e., for temperatures $T > T_c^f$. CCFs for Ising-type systems in the ordinary surface UC (including crossover effects to the normal surface UC) have been previously studied within the grand canonical ensemble in Refs. [22–30].

In Sec. II, we define the general scaling variables required for the description of the universal critical properties and outline the scaling relations expected for the OP profile. We furthermore introduce the Landau-Ginzburg model which is analyzed in the remaining part of this study. The OP profile resulting from the Landau-Ginzburg model within mean-field theory is determined perturbatively in Sec. III and fully via numerical studies in Sec. IV. The associated relation between the total mass and the external bulk field is analyzed separately in Sec. V. In Sec. VI, the CCF is studied analytically within linearized MFT and numerically within full MFT, focusing on ensemble differences. In Sec. VII the predictions of MFT are compared to Monte Carlo (MC) simulations of the three-dimensional Ising model.

II. PRELIMINARIES

A. Scaling behavior

Here, we summarize the general scaling behavior expected for the OP profile and the CCF in a d -dimensional film of thickness L . In the following we focus on the so-called ordinary fixed point, at which $c = \infty$ and, accordingly, the dependence of the scaling functions on c drops out. The following finite-size scaling relations apply to isotropic systems with short-ranged interactions below the upper critical dimension $d = 4$ of the Ising universality class [31, 32]. The uni-

versal properties of a critical film are expected to be controlled by the following set of scaling variables:

$$\zeta \equiv z/L, \quad (2a)$$

$$x \equiv \left(\frac{L}{\xi_+^{(0)}} \right)^{1/\nu} t, \quad (2b)$$

$$B \equiv \left(\frac{L}{\xi_\mu^{(0)}} \right)^{\Delta/\nu} \mu, \quad (2c)$$

$$\mathcal{M} \equiv \left(\frac{L}{\xi_+^{(0)}} \right)^{\beta/\nu} \frac{\varphi}{\phi_t^{(0)}}, \quad (2d)$$

where

$$\varphi \equiv \frac{\Phi}{L} \quad (3)$$

is the mean mass density of the film, β , ν , and Δ are standard bulk critical exponents, and

$$t = \frac{T - T_c^b}{T_c^b} \quad (4)$$

is the reduced temperature relative to the bulk critical temperature T_c^b . In the case of a one-component fluid the external bulk field μ describes the deviation of the chemical potential from its critical value in the bulk, while for a binary liquid mixture, μ represents the deviation of the difference in the chemical potentials of the two species A and B from its bulk critical value: $\mu \equiv (\mu_A - \mu_B) - (\mu_{A,c} - \mu_{B,c})$. The quantities $\xi_+^{(0)}$ and $\xi_\mu^{(0)}$ (as well as $\xi_-^{(0)}$, which we include here for completeness) denote non-universal amplitudes defined in terms of the (bulk) correlation length ξ_t at zero bulk field and ξ_μ at zero reduced temperature:

$$\xi_t = \xi_\pm^{(0)} |t|^{-\nu}, \quad \text{for } \mu = 0 \text{ and } t \rightarrow 0^\pm, \quad (5a)$$

$$\xi_\mu = \xi_\mu^{(0)} |\mu|^{-\nu/\Delta}, \quad \text{for } t = 0 \text{ and } \mu \rightarrow 0. \quad (5b)$$

The value of $\xi_\pm^{(0)}$ is different for $t \lesseqgtr 0$, but the amplitude ratio $U_\xi \equiv \xi_+^{(0)}/\xi_-^{(0)}$ forms the universal number $U_\xi \simeq 1.9$ in $d = 3$ and $U_\xi = \sqrt{2}$ in $d = 4$ spatial dimensions [33]. Except for Sec. IV, we focus on the supercritical regime and therefore in the scaling relations we use solely $\xi_+^{(0)}$. The non-universal amplitude $\phi_t^{(0)}$ is defined in terms of the bulk OP ϕ_b , which, near criticality, behaves as

$$\phi_{b,t} = \theta(-t) \phi_t^{(0)} |t|^\beta, \quad \text{for } \mu = 0 \text{ and } t \rightarrow 0, \quad (6a)$$

$$\phi_{b,\mu} = \text{sgn}(\mu) \phi_\mu^{(0)} |\mu|^{1/\delta}, \quad \text{for } t = 0 \text{ and } \mu \rightarrow 0, \quad (6b)$$

in the case of a vanishing external field μ and a vanishing reduced temperature t , respectively.

The OP profiles in the grand canonical and the canonical ensemble fulfill the following scaling relations [2, 3, 5, 32, 34]:

$$\phi^{(\text{gc})}(z, t, \mu, L) = \phi_t^{(0)} \left(\frac{L}{\xi_+^{(0)}} \right)^{-\beta/\nu} m^{(\text{gc})} \left(\frac{z}{L}, \left(\frac{L}{\xi_+^{(0)}} \right)^{1/\nu} t, \left(\frac{L}{\xi_\mu^{(0)}} \right)^{\Delta/\nu} \mu \right), \quad (7a)$$

$$\phi^{(\text{c})}(z, t, \varphi, L) = \phi_t^{(0)} \left(\frac{L}{\xi_+^{(0)}} \right)^{-\beta/\nu} m^{(\text{c})} \left(\frac{z}{L}, \left(\frac{L}{\xi_+^{(0)}} \right)^{1/\nu} t, \left(\frac{L}{\xi_+^{(0)}} \right)^{\beta/\nu} \frac{\varphi}{\phi_t^{(0)}} \right), \quad (7b)$$

where $m^{(\text{c,gc})}$ are the corresponding universal scaling functions. In order to simplify the notation, we henceforth drop the superscripts (c) and (gc) on ϕ and m . The scaling variable \mathcal{M} in Eq. (2d) is related to the scaling function m via

$$\mathcal{M} = \int_0^1 d\zeta m(\zeta). \quad (8)$$

The general scaling behavior of the CCF is discussed in Sec. VI. We remark that the scaling relations stated above apply for simple fluids with isotropic short-ranged interactions, so that two-scale factor universality holds. For a discussion of the influence of anisotropy as well as of long-ranged (van der Waals) interactions on the critical behavior we refer to Refs. [35–41].

B. Model and boundary conditions

We aim at determining the order parameter profile between two parallel plates, located at $z = 0, L$ and sub-

ject to the constraint of a specified total mass Φ [see Eq. (1) and recall that here and in the following Φ is considered per area A]. The canonical Landau-Ginzburg (LG) free energy functional for films, in units of $k_B T$ per transverse area A of the plates, is given by

$$\mathcal{F}_f^{(\text{c})}[\phi] \equiv \int_0^L dz \left[\frac{1}{2} (\partial_z \phi)^2 + \frac{1}{2} \tau \phi^2 + \frac{1}{4!} g \phi^4 \right] + [c_1 \phi^2(z=0) + c_2 \phi^2(z=L)]. \quad (9)$$

The integral represents the bulk contribution, whereas the terms $\propto c_1, c_2$ are surface enhancements giving rise to Robin-type boundary conditions [3] on ϕ — see Eq. (12) below. Within MFT, the coupling constants τ and g are given by $\tau = (\xi_+^{(0)})^{-2} t$ and $g = 6(\xi_+^{(0)} \phi_t^{(0)})^{-2}$, where t is the reduced temperature [Eq. (4)] and the amplitudes $\xi_+^{(0)}$ and $\phi_t^{(0)}$ are defined in Eqs. (5a) and (6a). Within MFT, one has $\xi_-^{(0)}/\xi_+^{(0)} = 1/\sqrt{2}$. Equilibrium states minimize Eq. (9), subject to the constraint in Eq. (1). In the grand canonical ensemble the LG functional for films (per $k_B T$ and area A) reads

$$\mathcal{F}_f^{(\text{gc})}([\phi]; \mu) \equiv \int_0^L dz \left[\frac{1}{2} (\partial_z \phi)^2 + \frac{1}{2} \tau \phi^2 + \frac{1}{4!} g \phi^4 - \mu \phi \right] + [c_1 \phi^2(z=0) + c_2 \phi^2(z=L)], \quad (10)$$

which is to be minimized with respect to ϕ , taking for the external bulk field (i.e., the chemical potential) μ a value such that Eq. (1) is obeyed. Minimization of the grand canonical energy functional leads to the Euler-Lagrange equation (ELE)

$$\partial_z^2 \phi - \tau \phi - \frac{g}{6} \phi^3 + \mu = 0, \quad (11)$$

subject to the boundary conditions

$$\partial_z \phi|_{z=0} = c_1 \phi(z=0), \quad \partial_z \phi|_{z=L} = -c_2 \phi(z=L), \quad (12)$$

induced by the surface enhancement terms. In what follows, we shall study the limits $c_1, c_2 \rightarrow \infty$, for which Dirichlet boundary conditions $\phi(z=0) = 0 = \phi(z=L)$ emerge.

Within MFT, the finite-size scaling variables defined in Eq. (2) turn into

$$x = L^2 \tau, \quad B = \sqrt{\frac{g}{6}} L^3 \mu, \quad m(\zeta) = \sqrt{\frac{g}{6}} L \phi(\zeta L), \quad \varphi = \Phi/L, \quad \text{and} \quad \mathcal{M} = \sqrt{\frac{g}{6}} L \varphi, \quad (13)$$

in terms of which $\mathcal{F}_f^{(\text{gc})}$ in Eq. (10) can be expressed as

$$\mathcal{F}_f^{(\text{gc})}([m]; B) = \frac{\Delta_0}{L^3} \left\{ \int_0^1 d\zeta \left[\frac{1}{2}(m')^2 + \frac{1}{2}xm^2 + \frac{1}{4}m^4 - Bm \right] + [c_1 m^2(0) + c_2 m^2(1)] \right\}. \quad (14)$$

The non-universal amplitude Δ_0 is given by

$$\Delta_0 \equiv \left(\xi_+^{(0)} \phi_t^{(0)} \right)^2 = \frac{6}{g} \quad (15)$$

in terms of the amplitudes of the correlation length and the bulk OP [see Eqs. (6a) and (5a)]. We note that Δ_0 has the same dimension as L^{4-d} , while the film free energies in Eqs. (9) and (10), being defined per area A , have the dimension of $1/L^{d-1}$. The dimensionless form of the ELE, following from Eqs. (11) and (12), reads

$$m''(\zeta) - xm(\zeta) - m^3(\zeta) + B = 0, \quad (16)$$

with the corresponding Dirichlet boundary conditions (obtained in the limits $c_1, c_2 \rightarrow \infty$)

$$m(0) = m(1) = 0. \quad (17)$$

Equations (16) and (17) are independent of the plate separation L and the coupling constant g , because these variables can be scaled out such that they appear as prefactors in Eq. (14). In general, the dimensionless counterpart of g is fixed under renormalization-group flow, which requires to include fluctuations into the theory. Within MFT, g and Δ_0 can be related to experimentally accessible critical amplitudes via Eq. (15).

III. PERTURBATIVE MEAN FIELD ANALYSIS

In order to make analytical progress, we address the nonlinear term of the ELE in Eq. (16) perturbatively by introducing a parameter ϵ (eventually to be set to unity):

$$m''(\zeta) - xm(\zeta) - \epsilon m^3(\zeta) + B = 0. \quad (18)$$

This equation must be solved subject to the Dirichlet boundary conditions in Eq. (17) and under the constraint [Eq. (8)]

$$\int_0^1 d\zeta m(\zeta) = \mathcal{M}. \quad (19)$$

In a first step, we solve Eq. (18) without this constraint by carrying out perturbation theory in terms of powers of ϵ , with the series expansions

$$\begin{aligned} m &= \sum_{i \geq 0} \epsilon^i m_i = m_0 + \epsilon m_1 + \epsilon^2 m_2 + \dots, \\ B &= \sum_{i \geq 0} \epsilon^i B_i = B_0 + \epsilon B_1 + \epsilon^2 B_2 + \dots \end{aligned} \quad (20)$$

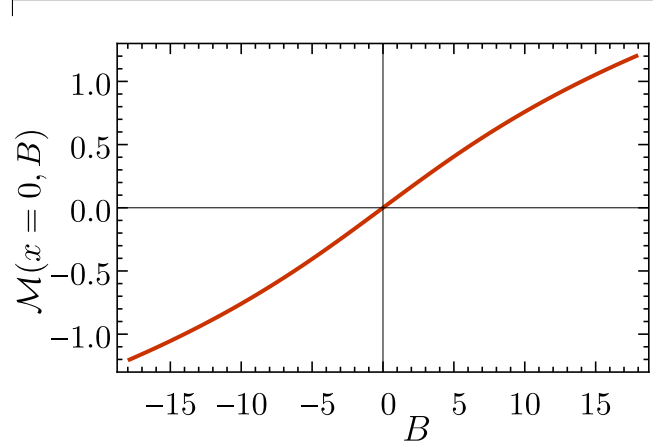


FIG. 1. The total mass as a function of the bulk field B at the bulk critical temperature ($x = 0$), determined from the (non-perturbative) numerical solution of the unconstrained ELE in Eq. (18).

The boundary conditions from Eq. (17) hold for each term i . Concerning the expansion of the mass constraint in Eq. (19), we choose

$$\mathcal{M}_0 = \mathcal{M}, \quad \mathcal{M}_{i \geq 1} = 0, \quad (21)$$

where $\mathcal{M}_i = \int_0^1 d\zeta m_i(\zeta)$.

As a side remark, one infers from the structure of the ELE that, if $m(\zeta)$ is a solution of Eq. (18) with parameters x and B , then $-m(\zeta)$ will be a solution for the parameters x and $-B$. Thus, the total mass $\mathcal{M}(x, B)$ is an odd function of the bulk field B , i.e., $\mathcal{M}(x, B) = -\mathcal{M}(x, -B)$. This feature is illustrated in Fig. 1 for the full, numerical (non-perturbative) solution of Eq. (18), which must hold also at each perturbative order.

A. Solution at $\mathcal{O}(\epsilon^0)$

At this order, Eq. (18) yields

$$m_0'' = xm_0 - B_0, \quad (22)$$

with the solution

$$m_0(\zeta) = \frac{B_0}{x} \left[1 - \operatorname{sech} \left(\frac{\sqrt{x}}{2} \right) \cosh \left((\zeta - 1/2)\sqrt{x} \right) \right]. \quad (23)$$

In contrast to the case of critical adsorption considered in Ref. [15], the lowest order MFT solution for Dirichlet boundary conditions is well-behaved near the bulk critical point. This is revealed by a series expansion for small x , yielding $m_0(\zeta) \simeq \frac{1}{8}[B_0 - 4B_0(\zeta - 1/2)^2]$. By using Eq. (13), Eq. (23) can be written in terms of dimensional variables:

$$\phi_0(z) = \frac{\mu}{\tau} \left[1 - \operatorname{sech} \left(\frac{L\sqrt{\tau}}{2} \right) \cosh \left(\sqrt{\tau} \left(z - \frac{L}{2} \right) \right) \right], \quad (24)$$

which will be useful for the analysis presented in Sec. VI A.

Implementing now the constraint in Eq. (21) selects and fixes, at this order, the value $B_0 = \tilde{B}_0$:

$$\tilde{B}_0 = \frac{\mathcal{M}x^{3/2}}{\sqrt{x} - 2 \tanh \left(\frac{\sqrt{x}}{2} \right)} \rightarrow \begin{cases} 12\mathcal{M}, & x \rightarrow 0, \\ \mathcal{M}x, & x \rightarrow \infty, \end{cases} \quad (25)$$

where the last expression exhibits the asymptotic scaling behavior close to the bulk critical point and for thick films, respectively. Inserting Eq. (25) into Eq. (23) gives the contribution to the constrained order parameter at this order:

$$\tilde{m}_0(\zeta) = \frac{\mathcal{M}\sqrt{x} \left[1 - \operatorname{sech} \left(\frac{\sqrt{x}}{2} \right) \cosh \left((\zeta - 1/2)\sqrt{x} \right) \right]}{\sqrt{x} - 2 \tanh \left(\frac{\sqrt{x}}{2} \right)}. \quad (26)$$

The asymptotic scaling of this expression,

$$\tilde{m}_0(\zeta) \rightarrow \begin{cases} 3\mathcal{M}(\frac{1}{2} - 2(\zeta - \frac{1}{2})^2), & x \rightarrow 0, \\ \mathcal{M}, & x \rightarrow \infty, \end{cases} \quad (27)$$

shows that at bulk criticality the lowest order MFT contribution for Dirichlet boundary conditions is a parabolic profile. In turn, away from criticality, the (spatially constant) solution must vanish due to the boundary conditions, which shows that $\mathcal{M} \rightarrow 0$ if $x \rightarrow \infty$. Consequently, \tilde{B}_0 in Eq. (25) must also vanish away from criticality. Finally, expressing Eq. (26) in terms of dimensional variables, one finds the constrained profile

$$\tilde{\phi}_0(z) = \varphi \frac{1 - \operatorname{sech} \left(\frac{L\sqrt{\tau}}{2} \right) \cosh \left(\sqrt{\tau} \left(z - \frac{L}{2} \right) \right)}{1 - \frac{2 \tanh \left(\frac{L\sqrt{\tau}}{2} \right)}{L\sqrt{\tau}}}, \quad (28)$$

which indeed satisfies the relation $\int_0^L dz \tilde{\phi}_0(z) = \varphi L = \Phi$.

B. Solution at $\mathcal{O}(\epsilon^1)$

To linear order in ϵ , Eq. (18) gives

$$m_1'' = xm_1 + m_0^3 - B_1. \quad (29)$$

The solution of this differential equation vanishes in the limit $B \rightarrow 0$. (The full expression is cumbersome and is not shown here.) Implementing the constraint of Eq. (21), one finds the following corresponding specific expression $B_1 = \tilde{B}_1$:

$$\tilde{B}_1 = \frac{\tilde{B}_0^3 \operatorname{sech}^4 \left(\frac{\sqrt{x}}{2} \right)}{48x^3 \left(\sqrt{x} - 2 \tanh \left(\frac{\sqrt{x}}{2} \right) \right)} \times \left[108\sqrt{x} - 160 \sinh(\sqrt{x}) - 25 \sinh(2\sqrt{x}) + 96\sqrt{x} \cosh(\sqrt{x}) + 6\sqrt{x} \cosh(2\sqrt{x}) \right], \quad (30)$$

which exhibits the asymptotic scaling behavior

$$\tilde{B}_1 \rightarrow \begin{cases} \frac{72}{35}\mathcal{M}^3, & x \rightarrow 0, \\ \mathcal{M}^3, & x \rightarrow \infty. \end{cases} \quad (31)$$

From this the constrained profile for very small and very large x can be calculated:

$$\tilde{m}_1(\zeta) \rightarrow \begin{cases} -\frac{9\mathcal{M}^3}{8960} [3840(\zeta - 1/2)^8 - 5376(\zeta - 1/2)^6 + 3360(\zeta - 1/2)^4 - 656(\zeta - 1/2)^2 + 23], & x \rightarrow 0, \\ 0, & x \rightarrow \infty. \end{cases} \quad (32)$$

At bulk criticality, a polynomial solution obeying the boundary conditions in Eq. (17) is obtained. As it was the case for the contribution $\mathcal{O}(\epsilon^0)$, the constrained profile vanishes away from criticality.

The perturbative solution of the ELE to $\mathcal{O}(\epsilon^2)$ is reported in Appendix A.

IV. COMPARISON OF PERTURBATIVE MFT SOLUTIONS WITH EXACT AND NUMERICAL RESULTS

In this section we compare the leading perturbative solution at order $\mathcal{O}(\epsilon^0)$ with numerical solutions of the full, nonlinear ELE (18). In the case of zero external field, the full solution $m(\zeta)$ can be computed analytically (see Sec. IV A below). In Sec. IV B we consider the unconstrained solution $m(\zeta)$ for a given pair of parameters (x, B) , and compare it with $m_0(\zeta)$ given by Eq. (23). Therefore, in Sec. IV C we impose the constraint on the total mass and regard the corresponding solution $\tilde{m}(\zeta)$ as a function of the independent parameters (x, \mathcal{M}) . The latter is compared with $\tilde{m}_0(\zeta)$ as given by Eq. (26).

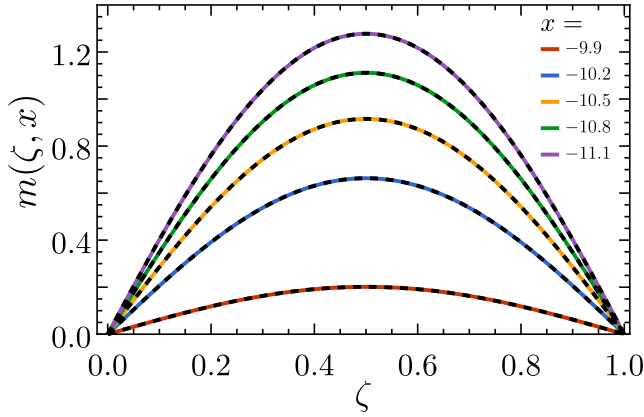


FIG. 2. OP profiles $m(\zeta, x)$ across the film in the grand canonical ensemble obtained for zero scaled bulk field, $B = 0$. The exact result from Eq. (36) (colored lines) is compared with the numerical solutions (black dashed lines) of the nonlinear MFT for several values of x below the film critical point, i.e., in the range $x < x_c^f$ [see Eq. (34)].

A. Exact analysis for $B = 0$ and location of the film critical point

For $B = 0$ an exact expression for the order parameter profile can be obtained in closed form in terms of elliptic functions [42]. According to Eq. (16), the associated ELE is

$$m''(\zeta) - xm(\zeta) - m^3(\zeta) = 0, \quad (33)$$

subject to the boundary conditions $m(0) = m(1) = 0$. Beside the trivial solution $m(\zeta) = 0$, there is a non-vanishing solution for $x \leq x_c^f$, where

$$x_c^f = -\pi^2 \simeq -9.87 \quad (34)$$

denotes the scaled reduced temperature (relative to the bulk critical point) of the film critical point. MC simulations of the Ising model [43] yield a value $x_c^f \simeq -7.6$ for the film critical point, while field theoretic renormalization group studies [44] predict $x_c^f \simeq -6.44$. Here and in the following, when considering the regime $t < 0$, i.e., $x < 0$, we define x as

$$x = \left(\frac{L}{\xi_-^{(0)}} \right)^{1/\nu} \frac{T - T_c^b}{T_c^b}. \quad (35)$$

One finds that

$$m_{\text{exact}}(\zeta) = 2\sqrt{2}kK(k^2) \operatorname{sn}(2K(k^2)\zeta; k^2), \quad (36)$$

where

$$K(k^2) = \int_0^1 \frac{du}{\sqrt{(1-u^2)(1-k^2u^2)}} \quad (37)$$

is the complete elliptic integral of the first kind, k is the elliptic modulus, determined implicitly by x through

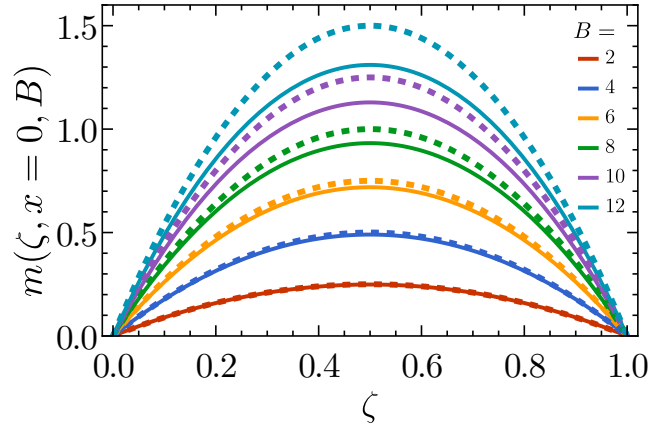


FIG. 3. The numerical solution $m(\zeta)$ (full curves) of the nonlinear MFT in the grand canonical ensemble is compared with $m_0(\zeta)$ (Eq. (23); dashed curves) for $x = 0$ and $B \in \{2, 4, 6, 8, 10, 12\}$. The discrepancy between the numerical and the truncated perturbative results grows as B increases, and its maximum occurs at the midpoint $\zeta = 1/2$ of the film.

$x = -4K^2(k^2)(1 + k^2)$, and sn is Jacobi's *elliptic sine* (see Refs. [45, 46] for more details). As shown in Fig. 2, the numerical solution of Eq. (33) perfectly matches the exact solution given in Eq. (36).

B. Unconstrained profiles

1. Profiles for $x = 0$

In Fig. 3, a comparison is shown of the unconstrained profiles obtained numerically with the perturbative approach at leading order. The perturbative solution $m_0(\zeta)$ [Eq. (23)] deviates significantly from the numerical solution for large values of the bulk field B , with the largest deviations being localized in the middle of the film (i.e., $\zeta = 1/2$). Close to the film boundaries at $\zeta = 0, 1$, the inaccuracy of the perturbative solution is mitigated by the fact that the Dirichlet boundary conditions are satisfied for all values of B .

2. Profiles for $x \neq 0$

The approach outlined above can be followed also for $x \neq 0$, and in principle the entire phase diagram can be explored. However, the same qualitative behavior encountered for $x = 0$ occurs also for $x \neq 0$. In general, the strongest inaccuracy is observed for $x < 0$ (as the phase-separating regime is approached) and for large values of B (where nonlinear effects become more dominant due to the term $\propto m^3$ in the ELE).

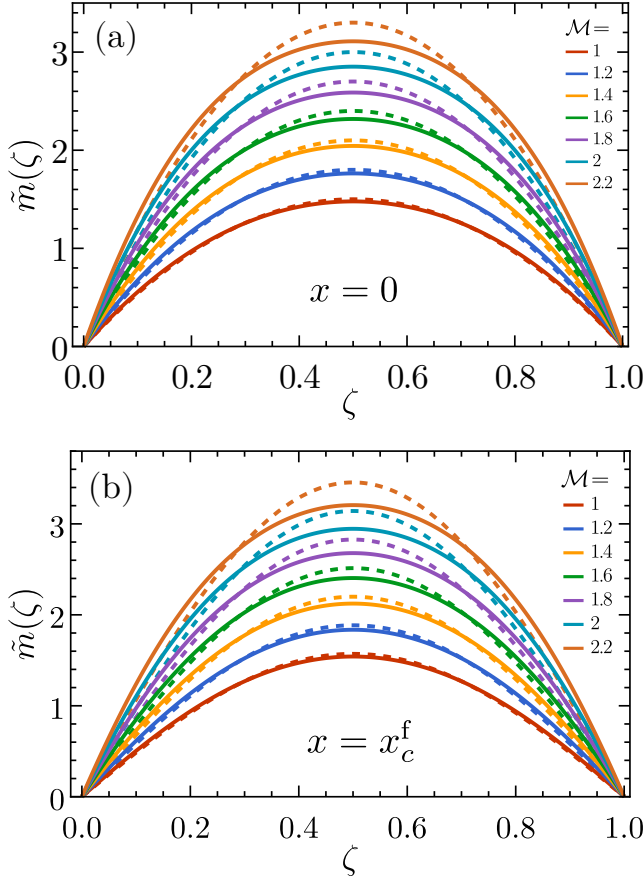


FIG. 4. The numerical solution $\tilde{m}(\zeta)$ (continuous curves) of the nonlinear MFT in the canonical ensemble is compared with $\tilde{m}_0(\zeta)$ (Eq. (26), dashed curves) for $x = 0$ (a) and $x = x_c^f$ [see Eq. (34)] (b), for various values of the imposed mass \mathcal{M} .

C. Constrained profiles at $x = 0$ and $x = x_c^f$

Here we consider the constrained profiles obtained by numerically solving the ELE [Eq. (16)] and compare them with the first-order perturbative solution [Eq. (26)]. In Fig. 4, the two cases $x = 0$ and $x = x_c^f = -\pi^2$ [Eq. (34)] are examined, where the latter corresponds to the film critical point. It is interesting to note that for $x = x_c^f$ the perturbative profile is not singular, but reduces to a particularly compact form:

$$\lim_{x \rightarrow x_c^f} \tilde{m}_0(\zeta) = \frac{\pi \mathcal{M}}{2} \sin(\pi \zeta). \quad (38)$$

V. PHASE DIAGRAMS, EQUATION OF STATE, AND SCALING

Here we explore the magnetization phase diagram, the equation of state $\mathcal{M}(x, B)$, and, in particular, we compare the film behavior with the one corresponding to the

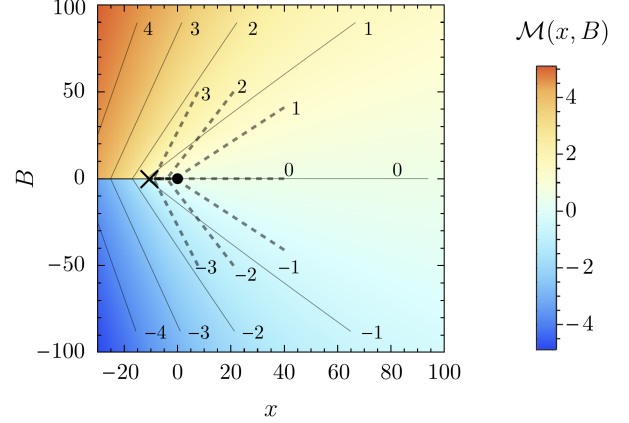


FIG. 5. Phase diagram and equation of state of a film with Dirichlet boundary conditions obtained numerically within nonlinear MFT. The color code indicates the value of the mass as a function of the scaled bulk field B and the scaled reduced temperature x . Solid lines are iso- \mathcal{M} lines for the film, while overlaid dashed lines correspond to the bulk system. The cross (\times) indicates the film critical point ($x = x_c^f = -\pi^2$, Eq. (34)), and the dot (\bullet) the bulk critical point ($x = 0$).

bulk. Exact numerical results are discussed in Sec. V A, while the validity of the perturbative MFT results is studied in Sec. V B. In Sec. V C we show that the near-critical behavior of the mass can be captured by simple scaling arguments. This scaling behavior can even be applied to the order parameter profiles themselves, as will be discussed in Sec. V D.

A. Exact numerical results for the mass

While the nonlinear ELE in Eq. (18), subject to Dirichlet boundary conditions, can be solved by standard numerical methods for $x > x_c^f$ (i.e., above phase separation in the film) and for sufficiently small B (for which nonlinear effects are not too strong), these methods typically become inaccurate outside these regimes, where gradients of the profile can be large. This issue can be addressed by solving the ELE via the so-called symplectic integration method [15, 47, 48], which, by construction, yields a spatially constant pressure in equilibrium. Essentially the ELE in Eq. (16) is equivalent to the Hamiltonian “equations of motion”, and the algorithm conserves the Hamiltonian density $\mathcal{H} = (m')^2/2 - xm^2/2 - m^4/4 + Bm$, which, in turn, allows one to directly extract the film pressure $p_f = (\Delta_0/L^4)\mathcal{H}$ (see, c.f., Eq. (63)). This method has the advantage that it avoids the (inaccurate) numerical computation of m' . The order parameter profile obtained this way for a pair (x, B) of scaling variables can be integrated numerically

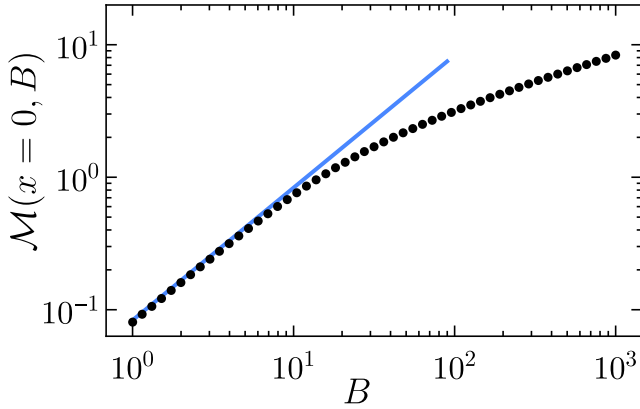


FIG. 6. Mass \mathcal{M} at the bulk critical point $x = 0$ as a function of the scaled bulk field B . The solid blue straight line represents the lowest order MFT result [Eq. (25)], while the black dots provide the numerical solution of the nonlinear MFT.

in order to determine the corresponding mass. The results of this procedure are shown in Fig. 5. The shift of the critical point in the film is clearly visible, as is the symmetry $\mathcal{M}(x, -B) = -\mathcal{M}(x, B)$. The super-imposed bulk diagram was obtained by solving Eq. (18), without the gradient term, for $m = \text{const}$.

B. Comparing exact and perturbative results for the mass

1. Mass as function of an external field at $x = 0$

The lowest order perturbative MFT solution for the mass [Eq. (25)] is linear in B at bulk T_c , i.e., $x = 0$. In Fig. 6 we compare this result (solid line) with the exact mass computed from the numerical solution of the nonlinear MFT (dots). The lowest order MFT result starts to deviate significantly from the exact result at $B \gtrsim 10$, whereas the numerical solution gradually approaches the bulk critical behavior $\mathcal{M} \propto B^{1/\delta}$ with $\delta = 3$ within MFT.

2. Mass as function of x with $B = 0$

In the absence of the external magnetic field one can use the exact solution (Eq. (36)) for the study of the mass:

$$\mathcal{M}(x, B = 0) = \int_0^1 d\zeta m_{\text{exact}}(\zeta, x). \quad (39)$$

The elliptic modulus $k = k(x)$ entering into the exact solution is the positive root of the implicit equation $-x = 4K^2(k^2)(1 + k^2)$, with x defined in Eq. (35).

The integration in Eq. (39) can be carried out in closed form by using elementary properties of elliptic functions [45, 46]:

$$\mathcal{M}(x, 0) = 2\sqrt{2} \tanh^{-1}(k(x)). \quad (40)$$

From this result one can easily extract the asymptotic behavior of the mass. In particular, we proceed to analyze Eq. (40) for (i) x close to film criticality T_c^f , i.e., for $x \lesssim x_c^f = -\pi^2$, and for (ii) extreme subcritical temperatures $x \ll -1$.

(i) $x \lesssim x_c^f$: It is convenient to parametrize the deviation from the critical point as

$$x = -\pi^2(1 + t^f), \quad (41)$$

where $t^f = (T_c^f - T)/(T_c^b - T_c^f)$ is the film-analogue of the bulk reduced temperature t as introduced in Eq. (4). We note that for $T = T_c^f$ from Eq. (35) we have $x = x_c^f = (L/\xi_-^{(0)})^{1/\nu}(T_c^f - T_c^b)/T_c^b$, while instead at $T = T_c^b$ we recover $x = 0$, as expected. It follows furthermore that $T_c^f(L \rightarrow \infty)/T_c^b = 1 - \pi^2(L/\xi_-^{(0)})^{-1/\nu}$. We focus on the regime $t^f \rightarrow 0^+$. Since in this limit $x \rightarrow -(\pi^2)^-$ (see Eq. (41)), the implicit equation $-x = 4K^2(k^2)(1 + k^2)$ can be substituted by its Taylor expansion around the desired value of $k = 0$. The corresponding small-modulus expansion of the complete elliptic integral $K(k^2)$ is $K(k^2) = \frac{\pi}{2} \left(1 + \frac{k^2}{4} + \frac{9}{64}k^4 + \mathcal{O}(k^6)\right)$, which implies the following expression for t^f :

$$t^f = \frac{3}{2}k^2 + \frac{27}{32}k^4 + \frac{39}{64}k^6 + \mathcal{O}(k^8). \quad (42)$$

The solution $(t^f, k) = (0, 0)$, corresponding to $(x, k) = (-\pi^2, 0)$, is trivially reproduced. For $t^f \rightarrow 0^+$, Eq. (42) gives, to leading order, $k = \sqrt{\frac{2}{3}t^f}$, which is valid for x approaching $-\pi^2$ from below. Higher order corrections can be obtained by iterating this procedure. Inserting this result into Eq. (39) and using the fact that $\tanh^{-1}(k \rightarrow 0) = k + \mathcal{O}(k^3)$, one obtains the following scaling behavior:

$$\mathcal{M}(x, 0) \simeq \frac{4}{\sqrt{3}}(t^f)^\beta, \quad t^f \rightarrow 0^+ \text{ or } x \rightarrow (-\pi^2)^-, \quad (43)$$

with the exponent $\beta = \frac{1}{2}$. Equation (43) is valid in the asymptotic regime $t^f \rightarrow 0^+$ where successive corrections $\sim (t^f)^{\hat{\beta}}$, characterized by an exponent $\hat{\beta} > \beta$, vanish faster than $(t^f)^\beta$.

(ii) $x \ll -1$: Since $-x \gg 1$, the roots of $x(k)$ accumulate towards $k = 1^-$. Writing $k = 1 - \epsilon$ for certain $\epsilon \rightarrow 0^+$, one has $\tanh^{-1}(1 - \epsilon) = \frac{1}{2} \ln \frac{2}{\epsilon} + \frac{1}{2}p_n(\epsilon) + \mathcal{O}(\epsilon^{n+1})$, where $p_n(\epsilon)$ is a polynomial in ϵ of degree n . Hence for large $|x|$ the mass is approximately given by $\mathcal{M}(x, 0) \simeq \sqrt{2} \ln \frac{2}{\epsilon} + \sqrt{2}p(\epsilon)$. In order to identify the small parameter ϵ in terms of x ,

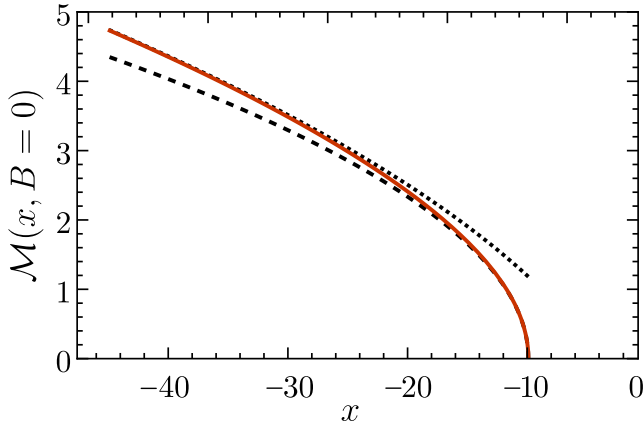


FIG. 7. Mass \mathcal{M} in a film with Dirichlet boundary conditions for $B = 0$ as a function of x , as given by the exact MFT expression in Eq. (40) (red solid curve). The asymptotic behavior described in Eq. (43) (dashed curve) and in Eq. (44) (dotted curve) agree with the exact expression for $x = x_c^f \approx -9.87$ and for large values of $-x$, respectively.

we note that if the elliptic modulus approaches unity, $K(k^2) = -\frac{1}{2} \ln \left(\frac{1-k^2}{16} \right) [1 + \mathcal{O}(1-k)]$, so that the implicit equation for $k(x)$ exhibits the asymptotic behavior $k(x) \simeq 1 - 8e^{-\sqrt{-x}/2} = 1 - \epsilon$. Accordingly, the mass is $\mathcal{M}(x, 0) = \sqrt{-x} - 2\sqrt{2} \ln 2 + \sqrt{2}p(\epsilon)$, where the last term is negligible because $\epsilon \rightarrow 0$ and $p(0) = 0$. This renders the asymptotic result

$$\mathcal{M}(x, 0) \simeq \sqrt{-x} - 2\sqrt{2} \ln 2, \quad x \rightarrow -\infty. \quad (44)$$

To summarize, we have derived the analytical expression of the mass \mathcal{M} in the absence of an external field, and its asymptotic behavior close to film criticality ($x \lesssim x_c^f = -\pi^2$) and far from criticality in the two-phase region ($x \ll -1$). As shown in Fig. 7, the approximate expressions agree well with the analytical result in Eq. (40).

C. Widom scaling for the mass

It is well known [42, 49] and explicitly demonstrated in Sec. IV A, that in the film geometry the presence of two confining walls induces a shift of the bulk critical point from $x_c^b = 0$ to $x_c^f = -\pi^2$. In the present section we discuss in detail the mean-field critical behavior around x_c^f , resulting from Eq. (18).

It is useful to recall the essential ideas of the static scaling hypothesis, as originally formulated by Widom [50, 51]. The film critical point is located at $(t^f, B) = (0, 0)$, where t^f [see Eq. (41)] is the reduced temperature of the film relative to T_c^f . Instead of considering the order parameter profile inside the film, here we are

interested in the mass $\mathcal{M}(t^f, B) = \mathcal{M}(x(t^f), B)$. In the critical region of the film, for a vanishing bulk field B one expects the scaling behavior

$$\mathcal{M}(t^f, B = 0) = \begin{cases} 0, & t^f < 0 \\ \pm \mathcal{C}_{t^f} |t^f|^\beta, & t^f > 0. \end{cases} \quad (45)$$

We note that, according to Eq. (41), $t^f < 0$ [$t^f > 0$] corresponds to $x > x_c^f$ [$x < x_c^f$]. The critical isotherm follows as

$$\mathcal{M}(t^f = 0, B) = \mathcal{C}_B \text{sign}(B) |B|^{1/\delta}. \quad (46)$$

The above relations can be considered as a definition of the critical exponents β and δ and of the non-universal amplitudes \mathcal{C}_t and \mathcal{C}_B . According to the scaling hypothesis, in the near-critical region around T_c^f the equation of state fulfills a homogeneity relation of the form

$$\mathcal{M}(t^f, B) = \begin{cases} (-t^f)^\beta \mathcal{U}_- (B/(-t^f)^\Delta), & t^f < 0, \\ (t^f)^\beta \mathcal{U}_+ (B/(t^f)^\Delta), & t^f > 0, \end{cases} \quad (47)$$

where \mathcal{U}_\pm are a pair of universal scaling functions and $\Delta = \beta\delta$ is called the *gap exponent* [51, 52]. Various sections of the phase diagram in the scaling region lead to curves of the type shown in Fig. 8(a). A suitable rescaling of the thermodynamic variables t and B as prescribed by Eqs. (45) and (46) results in a data collapse onto two single master curves corresponding to the scaling functions \mathcal{U}_\pm (see Fig. 8(b)). In the previous subsection we have established Eq. (45) in the form of Eq. (43), leading to $\beta = \frac{1}{2}$ and to the non-universal amplitude $\mathcal{C}_{t^f} = \frac{4}{\sqrt{3}}$. On the other hand, the results of the complete numerical analysis, shown in Fig. 8, confirm Eq. (46); in fact the critical isotherm in the scaling region near x_c^f can be approximated well by Eq. (46) with the critical exponent $\delta = 3$ and the non-universal amplitude $\mathcal{C}_B \simeq 0.76$. We thus recover $\Delta = \frac{3}{2}$ for the gap exponent and obtain an excellent data collapse.

To summarize, our analytical and numerical analysis recovers the expected mean field critical exponents for the film critical point. We remark that the maximum value of the critical profile (in the center of the film) has the same scaling behavior as the total mass, $m(\zeta = \frac{1}{2}; x_c^f, B) = \hat{\mathcal{C}}_B \text{sign}(B) |B|^{1/\delta}$, with $\hat{\mathcal{C}}_B \simeq 1.19$ and $\delta = 3$.

This analysis reveals explicitly that, as expected, within MFT the bulk transition in spatial dimension d exhibits the same scaling behavior and the same critical exponents as its counterpart in the film which, asymptotically, behaves as an effectively $(d-1)$ -dimensional system. The inability to capture this actual dimensional crossover is a well-known shortcoming of many analytical approaches, i.e., MFT and beyond [2, 4, 53, 54] (see, however, Refs. [41, 55]), whereas simulations can deal with this issue successfully.

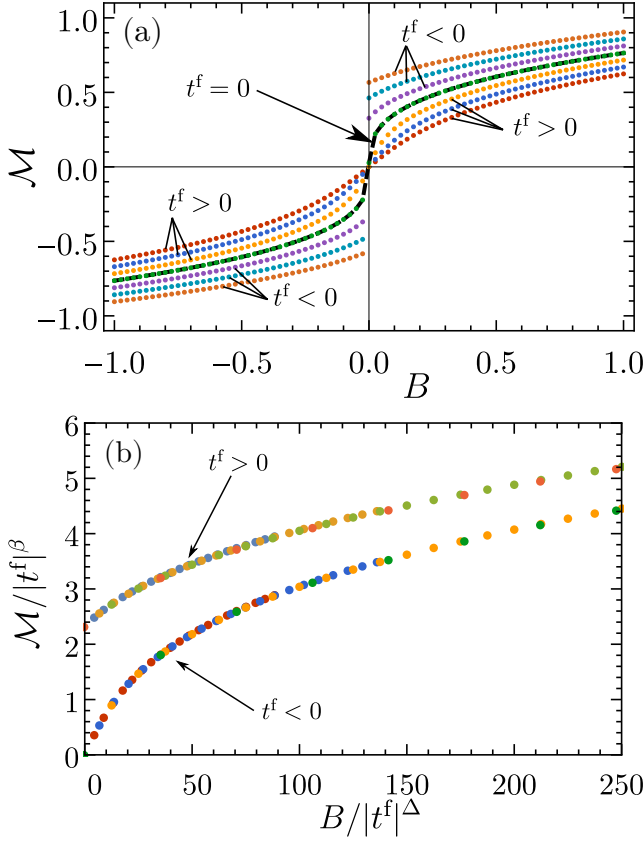


FIG. 8. (a) A section of the equation of state around the film critical point in the phase diagram. The critical isotherm corresponding to $t^f = 0$ [see Eq. (46)] is shown by the dashed black curve, while symbols represent numerical data. (b) Test of the scaling hypothesis [Eq. (47)] for data contained in panel (a). The points corresponding to the “supercritical” regime ($t^f < 0$) collapse onto the scaling function \mathcal{U}_- , while data for the “subcritical” regime ($t^f > 0$) collapse onto \mathcal{U}_+ .

D. Magnetization profiles in the near-critical region: insights from Widom scaling

Here we consider the case $B = 0$ and $x \lesssim x_c$. Since at criticality the profile vanishes, the ELE in Eq. (18) in the vicinity of the film critical point, i.e.,

$$m''(\zeta) - x_c^f m(\zeta) - m^3(\zeta) = 0, \quad (48)$$

can be approximated by the linearized equation

$$m''(\zeta) + \pi^2 m(\zeta) = 0, \quad (49)$$

because the cubic term is smaller than the linear terms. Equation (49) with Dirichlet boundary conditions is solved by

$$m_{\text{lin}}(\zeta) = \mathcal{A} \sin(\pi\zeta). \quad (50)$$

However, the amplitude \mathcal{A} cannot be fixed by Eq. (49), because the cubic term has been neglected. Nonetheless, we can determine \mathcal{A} by considering a suitable limit

of the exact solution. For $x \rightarrow -\pi^2$ we can use the reduced temperature $t^f \rightarrow 0$ from Eq. (41). We recall that within this limit the elliptic modulus is $k = \sqrt{\frac{2}{3}t^f}$ and that for vanishing k^2 the Jacobi elliptic function $\text{sn}(w; k^2 \rightarrow 0) \rightarrow \sin(w)$ reduces to a standard sine function. Therefore in the limit $t^f \rightarrow 0^+$ Eq. (36) produces exactly

$$m(\zeta, x \lesssim x_c^f, B = 0) = \frac{2\pi\sqrt{t^f}}{3} \sin(\pi\zeta). \quad (51)$$

Spatial integration yields the mass $\mathcal{M}(x, B = 0) = 4\left(\frac{t^f}{3}\right)^{1/2}$ for $x \rightarrow x_c^f$. The behavior of the scaled bulk field B is less obvious. In the previous section we noted a scaling behavior for the maximum value of the magnetization profiles, namely $m(\zeta = 1/2, B) \sim B^{1/3}$. The same behavior extends, with remarkably good agreement with the numerical results of Fig. 3, also to $\zeta \neq 1/2$. We find that Eq. (51) follows an analogous scaling, i.e.,

$$m(\zeta, x = x_c^f, B \simeq 0) = \hat{\mathcal{C}}_B B^{1/3} \sin(\pi\zeta). \quad (52)$$

Combining Eq. (51) and Eq. (52), in the scaling region around the film critical point we have

$$m(\zeta, x \lesssim x_c^f, B \simeq 0) = (t^f)^\beta \Phi\left(\frac{B}{(t^f)^\Delta}\right) \sin(\pi\zeta), \quad (53)$$

with a scaling function Φ . Since $\int_0^1 d\zeta \sin(\pi\zeta) = \frac{2}{\pi}$, one has

$$\mathcal{M}(x \simeq x_c, B \simeq 0) = (t^f)^\beta \Psi\left(\frac{B}{(t^f)^\Delta}\right), \quad (54)$$

where $\Psi(u) = (2/\pi)\Phi(u)$, so that Eq. (47) is recovered, for which we identify $\Psi(u)$ as $\mathcal{U}_+(u)$. Thus, the scaling functions computed for the mass equation of state in Fig. 8 capture well the spatially integrated order parameter profiles in the near-critical region.

VI. CRITICAL CASIMIR FORCE

In this section we study the critical Casimir force (CCF) in the grand canonical and the canonical ensemble, for a film subject to Dirichlet boundary conditions. We therefore briefly recall the general definitions and protocols for computing the CCF, as set out in Sec. III of Ref. [15].

In general, the equilibrium CCF \mathcal{K} provides the derivative of the residual free energy, or, in terms of the stress tensor, quantifies the change of the free energy of the film upon shifting the position of the boundaries. In the first case, one has

$$\mathcal{K} = -\frac{d\mathcal{F}_{\text{res}}}{dL}, \quad (55)$$

where we have decomposed the free energy of the film according to

$$\mathcal{F}_f = L(-p_b) + f_s + \mathcal{F}_{\text{res}}, \quad (56)$$

in terms of the bulk pressure p_b , the surface free energy f_s , and the residual free energy \mathcal{F}_{res} (all per transverse area A and $k_B T$). Generally, the bulk term scales

$\propto L$ and the surface term $\propto L^0$, while the residual terms vanish exponentially for $L \rightarrow \infty$ (see, e.g., Refs. [15, 32]). We remark that for realistic fluid films, long-ranged van der Waals forces provide algebraically decaying non-universal contributions to the residual free energy [35, 37, 38, 56]. In the present study, we consider only the universal critical Casimir contribution.

In the second case, the CCF is the difference between the film pressure $p_f = -d\mathcal{F}_f/dL$ and the pressure of the surrounding bulk medium in which the film is immersed:

$$\mathcal{K} = p_f - p_b. \quad (57)$$

The bulk pressure is naturally defined as

$$p_b = \lim_{L \rightarrow \infty} p_f, \quad (58)$$

where the limit is performed by keeping fixed the relevant thermodynamic control parameters (i.e., the chemical potential μ for the grand canonical ensemble, and the mass density $\varphi = \Phi/L$ for the canonical ensemble) [57].

The CCF (per transverse area A and $k_B T$) in the grand canonical and the canonical ensemble takes the following scaling form [2, 5, 15]:

$$\mathcal{K}^{(\text{gc})}(t, \mu, L) = L^{-d} \Xi^{(\text{gc})} \left(\left(\frac{L}{\xi_+^{(0)}} \right)^{1/\nu} t, \left(\frac{L}{\xi_\mu^{(0)}} \right)^{\Delta/\nu} \mu \right), \quad (59a)$$

$$\mathcal{K}^{(\text{c})}(t, \varphi, L) = L^{-d} \Xi^{(\text{c})} \left(\left(\frac{L}{\xi_+^{(0)}} \right)^{1/\nu} t, \left(\frac{L}{\xi_\varphi^{(0)}} \right)^{\beta/\nu} \frac{\varphi}{\phi_t^{(0)}} \right), \quad (59b)$$

where $\Xi^{(\text{gc})}$ and $\Xi^{(\text{c})}$ are scaling functions, which will be determined below for $t = (T - T_c^b)/T_c^b > 0$ and within MFT, whereby we take the values of the critical exponents pertaining to $d \geq 4$ spatial dimensions. The scaling relation in Eq. (59) expresses the two-scale factor universality [31, 32] valid for simple fluids below the upper critical dimension $d = 4$. Within MFT, the scaling functions $\Xi^{(\text{c}, \text{gc})}$ acquire an *a priori* undetermined prefactor Δ_0 involving the coupling constant g [Eq. (15)]. Accordingly, we shall present our results within MFT in terms of *reduced* scaling functions $\Xi^{(\text{c}, \text{gc})}/\Delta_0$.

Instead of using Eq. (58), the film pressure can equivalently be obtained from the stress tensor T_{ij} :

$$p_f = T_{zz}[\phi_{\text{eq}}] = -\frac{d}{dL} \mathcal{F}_f[\phi_{\text{eq}}], \quad (60)$$

where $T_{zz}[\phi_{\text{eq}}]$ is computed from the order parameter profile minimizing \mathcal{F}_f (Eqs. (9) and (10)). Note that here we have assumed the boundaries of the film to be normal to the z -direction. Analogously, the bulk pressure can be obtained from the corresponding bulk order parameter at equilibrium, $p_b = T_{zz}(\phi_b)$. Therefore Eq. (57) allows one to compute \mathcal{K} without explicitly evaluating derivatives of free energy functionals. In the grand canonical ensemble, the definitions of \mathcal{K} in Eqs. (55) and (57) yield equivalent results, whereas differences may appear due to additional surface contributions in the canonical ensemble [15]. We recall that, in thermal equilibrium, $T_{zz}[\phi_{\text{eq}}]$ is in general independent of z .

A core result of Ref. [15] is that the stress tensor in the canonical ensemble can be computed using a grand canonical stress tensor in which the chemical potential takes the value $\mu = \tilde{\mu}(\Phi)$, satisfying the mass constraint in Eq. (1),

$$T_{ij}^{(\text{c})}[\phi_{\text{eq}}] = T_{ij}^{(\text{gc})}([\phi_{\text{eq}}]; \mu = \tilde{\mu}), \quad (61)$$

in terms of the solution ϕ_{eq} of the ELE. By construction, this yields equal film pressures in the two ensembles, $p_f^{(\text{c})}[\phi_{\text{eq}}] = p_f^{(\text{gc})}([\phi_{\text{eq}}]; \tilde{\mu})$. In the grand canonical ensemble, the mean field stress tensor corresponding to the free energy functional in Eq. (10) is [2]

$$\begin{aligned} T_{ij}^{(\text{gc})}([\phi_{\text{eq}}]; \mu) &= (\partial_i \phi_{\text{eq}})(\partial_j \phi_{\text{eq}}) \\ &- \delta_{ij} \left[\frac{1}{2} \sum_k (\partial_k \phi_{\text{eq}})(\partial_k \phi_{\text{eq}}) + \frac{1}{2} \tau \phi_{\text{eq}}^2 + \frac{1}{4!} g \phi_{\text{eq}}^4 - \mu \phi_{\text{eq}} \right], \end{aligned} \quad (62)$$

giving rise to the film pressure

$$p_f^{(c,gc)} = T_{zz}^{(c,gc)} = \frac{1}{2}(\partial_z \phi_{eq})^2 - \frac{1}{2}\tau\phi_{eq}^2 - \frac{1}{4!}g\phi_{eq}^4 + \tilde{\mu}\phi_{eq} \\ = \frac{\Delta_0}{L^4} \left[\frac{1}{2}(\partial_\zeta m_{eq})^2 - \frac{1}{2}xm_{eq}^2 - \frac{1}{4}m_{eq}^4 + \tilde{B}m_{eq} \right], \quad (63)$$

where the dimensionless variables from Eq. (13) have been re-introduced; Δ_0 is given by Eq. (15). In turn, the bulk pressure in the grand canonical ensemble,

$$p_b^{(gc)}(\mu_b^{(gc)}) = \frac{1}{2}\tau\phi_b^2 + \frac{1}{8}g\phi_b^4, \quad (64)$$

is obtained by solving the bulk equation of state (i.e., the ELE without gradient terms),

$$\tau\phi_b + \frac{1}{6}g\phi_b^3 = \mu_b^{(gc)} = \mu, \quad (65)$$

in order to find the spatially constant solution ϕ_b , and to insert it into Eq. (61). By virtue of the grand canonical coupling between film and bulk, the chemical potential μ here is the same as for the film.

In contrast, in the canonical ensemble, the film and the bulk system are constrained to have the same mass density φ , which gives rise to the following canonical bulk pressure:

$$p_b^{(c)}(\phi_b) = \frac{1}{2}\tau\phi_b^2 + \frac{1}{8}g\phi_b^4, \quad \text{with} \quad \begin{cases} \phi_b = \pm\phi_{b,eq}, & \tau < 0 \quad \text{and} \quad -\phi_{b,eq} \leq \varphi \leq \phi_{b,eq}, \\ \phi_b = \varphi, & \text{otherwise,} \end{cases} \quad (66)$$

where $\phi_{b,eq}$ denotes the OP minimizing the LG functional in Eq. (9). The chemical potential corresponding to the bulk system of mass density φ is

$$\mu_b^{(c)} = \begin{cases} 0, & \tau < 0 \quad \text{and} \quad -\phi_{b,eq} \leq \varphi \leq \phi_{b,eq}, \\ \tau\varphi + \frac{1}{6}g\varphi^3, & \text{otherwise.} \end{cases} \quad (67)$$

In what follows, we shall focus on the region $\tau > 0$, i.e., we avoid bulk phase separation, so that the bulk pressure can be directly obtained as $p_b^{(c)}(\phi_b) = \frac{1}{2}\tau\varphi^2 + \frac{1}{8}g\varphi^4$.

As stated, the film pressures are equal in the grand canonical and the canonical ensembles. However, due to the different thermodynamic coupling of film and bulk outlined above, the CCF \mathcal{K} can differ in the respective ensembles. Indeed, this has been reported in Ref. [15] for the case of critical adsorption whereas here we investigate the CCFs for films with Dirichlet boundary conditions. We proceed by using the linear MFT results from Sec. III in order to compute the CCF using the stress tensor in Sec. VIA. These perturbative expressions are compared with exact numerical MFT results for the canonical and grand canonical scaling functions of the CCF. In Sec. VIC the CCF is computed directly by differentiating the free energy functionals, which are expressed in terms of the perturbatively computed OP profiles.

A. CCF within linear MFT deduced from the stress tensor

We employ the stress tensor in Eq. (63) in order to compute the film pressure from the order parameter profiles determined in Sec. III. In the grand canonical case, T_{zz} is determined in terms of the unconstrained OP in the presence of the external field, i.e., for fixed μ . The canonical pressure can be obtained analogously by using the constrained profile $\bar{\phi}$, where now $\tilde{\mu}(\varphi = \Phi/L)$ is the constraint-induced chemical potential guaranteeing a certain mass density φ . Rewriting Eq. (63) as

$$p_f^{(c,gc)} = \frac{\Delta_0}{L^4} \mathcal{T} \quad (68)$$

and inserting the expansion of m in terms of powers of ϵ as defined in Eqs. (18) and (20), we find the lowest orders of $\mathcal{T} = \mathcal{T}_0 + \epsilon\mathcal{T}_1 + \dots$:

$$\mathcal{T}_0 = \frac{1}{2}(\partial_\zeta \tilde{m}_0)^2 - \frac{\tilde{m}_0^2 x}{2} + \tilde{B}_0 \tilde{m}_0, \\ \mathcal{T}_1 = (\partial_\zeta \tilde{m}_0)(\partial_\zeta \tilde{m}_1) - \tilde{m}_0 \tilde{m}_1 x - \tilde{m}_0^3 \tilde{m}_1 + \tilde{B}_0 \tilde{m}_1 + \tilde{B}_1 \tilde{m}_0. \quad (69)$$

At lowest order we have implicitly neglected the ϕ^4 term in the free energy [and thus also the quartic term in Eq. (63)], which explains the absence of this term in the expression for \mathcal{T}_0 .

1. Grand canonical CCF

Using B instead of B_0 and inserting the linear MFT solution from Eq. (23) into Eqs. (68) and (69), we find

$$\mathcal{T}_0^{(\text{gc})} = \frac{B^2 \tanh^2\left(\frac{\sqrt{x}}{2}\right)}{2x}. \quad (70)$$

Upon rescaling to dimensional variables via Eq. (13), we identify the corresponding film pressure

$$(p_f^{(\text{gc})})_0 = \frac{\mu^2}{2\tau} \tanh^2\left(\frac{L\sqrt{\tau}}{2}\right). \quad (71)$$

The corresponding bulk limit, taken with μ fixed, is

$$(p_b^{(\text{gc})})_0 = \frac{\mu^2}{2\tau}. \quad (72)$$

The CCF can now be computed by using Eq. (57):

$$\mathcal{K}_0^{(\text{gc})} = -\frac{\mu^2}{\tau[1 + \cosh(L\sqrt{\tau})]}. \quad (73)$$

From Eq. (25), the chemical potential corresponding to the mass constraint follows as

$$\tilde{\mu} = \frac{\tau\varphi}{1 - \frac{2}{L\sqrt{\tau}} \tanh\left(\frac{L\sqrt{\tau}}{2}\right)}, \quad (74)$$

which, together with Eq. (73), gives

$$\mathcal{K}_0^{(\text{gc})} = -\frac{\tau\varphi^2}{(1 + \cosh(L\sqrt{\tau})) \left(1 - \frac{2 \tanh(L\sqrt{\tau}/2)}{L\sqrt{\tau}}\right)^2}. \quad (75)$$

According to Eq. (59a) (with $d = 4$), the reduced scaling function of the CCF results as

$$\frac{\Xi^{(\text{gc})}}{\Delta_0} = -\frac{\mathcal{M}^2 x^2}{(1 + \cosh(\sqrt{x})) \left(\sqrt{x} - 2 \tanh\left(\frac{\sqrt{x}}{2}\right)\right)^2}. \quad (76)$$

Note that this scaling function diverges at bulk criticality:

$$\frac{\Xi^{(\text{gc})}(x \rightarrow 0)}{\Delta_0} \simeq -\frac{72\mathcal{M}^2}{x}. \quad (77)$$

This divergence is entirely due to the bulk pressure in Eq. (72) and can be considered as an artifact of linear MFT. (An analogous divergence occurs in the case of critical adsorption, see Ref. [15].) Far above T_c , the scaling function vanishes as

$$\frac{\Xi^{(\text{gc})}(x \gg 0)}{\Delta_0} \simeq 2\mathcal{M}^2 e^{-\sqrt{x}}, \quad (78)$$

which is intuitively expected, because the CCF is expected to vanish in the limit of thick films, i.e., $x = (L/\xi)^{1/\nu} \rightarrow \infty$.

2. Canonical CCF

In this case, the constrained linear mean-field profile from Eq. 26 yields

$$\mathcal{T}_0^{(c)} = \frac{\mathcal{M}^2 x^2 \tanh^2\left(\frac{\sqrt{x}}{2}\right)}{2 \left(\sqrt{x} - 2 \tanh\left(\frac{\sqrt{x}}{2}\right)\right)^2}, \quad (79)$$

which renders the corresponding film pressure (expressed in terms of dimensional variables, see Eq. (13))

$$(p_f^{(c)})_0 = \frac{\tau\varphi^2}{2} \frac{\tanh^2\left(\frac{L\sqrt{\tau}}{2}\right)}{\left(1 - \frac{2 \tanh(L\sqrt{\tau}/2)}{L\sqrt{\tau}}\right)^2}. \quad (80)$$

The same expression results upon inserting Eq. (74) into Eq. (71). In the canonical ensemble, the bulk limit of Eq. (80) is obtained by keeping a fixed mass density φ [see Eq. (58)],

$$(p_b^{(c)})_0 = \frac{\tau\varphi^2}{2}. \quad (81)$$

Subtracting Eq. (81) from Eq. (80) leads to the CCF in the canonical ensemble:

$$\mathcal{K}_0^{(c)} = \frac{\tau\varphi^2}{2} \left[\frac{\tanh^2\left(\frac{L\sqrt{\tau}}{2}\right)}{\left(1 - \frac{2 \tanh(L\sqrt{\tau}/2)}{L\sqrt{\tau}}\right)^2} - 1 \right], \quad (82)$$

which can be brought into the scaling form given in Eq. (59b) with the reduced scaling function

$$\frac{\Xi^{(c)}}{\Delta_0} = \frac{\mathcal{M}^2 x}{2} \left[\frac{\tanh^2\left(\frac{\sqrt{x}}{2}\right)}{\left(1 - \frac{2}{\sqrt{x}} \tanh\left(\frac{\sqrt{x}}{2}\right)\right)^2} - 1 \right]. \quad (83)$$

A comparison with the grand canonical CCF from Eq. (76) reveals that

$$\begin{aligned} \frac{\Xi^{(c)}}{\Delta_0} &= \frac{\Xi^{(\text{gc})}}{\Delta_0} + \frac{\mathcal{M}^2 x}{2} \left[\frac{\tanh^2\left(\frac{\sqrt{x}}{2}\right)}{\left(1 - \frac{2}{\sqrt{x}} \tanh\left(\frac{\sqrt{x}}{2}\right)\right)^2} - 1 \right] \\ &= -\frac{\mathcal{M}^2 x^2}{(1 + \cosh(\sqrt{x})) \left(\sqrt{x} - 2 \tanh\left(\frac{\sqrt{x}}{2}\right)\right)^2} \\ &\quad + \frac{\mathcal{M}^2 x}{2} \left[\frac{\tanh^2\left(\frac{\sqrt{x}}{2}\right)}{\left(1 - \frac{2}{\sqrt{x}} \tanh\left(\frac{\sqrt{x}}{2}\right)\right)^2} - 1 \right]. \end{aligned} \quad (84)$$

Different from the grand canonical scaling function [Eq. (76)], the canonical one attains a finite value at bulk criticality:

$$\frac{\Xi^{(c)}(x \rightarrow 0)}{\Delta_0} \simeq 18\mathcal{M}^2. \quad (85)$$

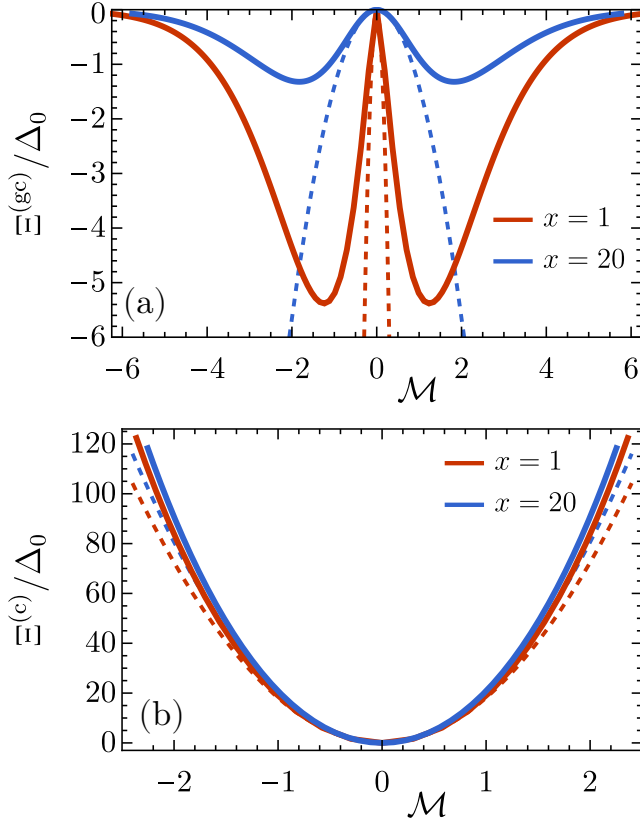


FIG. 9. The reduced scaling functions $\Xi^{(gc)}/\Delta_0$ (a) and $\Xi^{(c)}/\Delta_0$ (b) for the CCF in the grand canonical and canonical ensembles, respectively. Solid lines indicate the results obtained numerically within nonlinear MFT, while dashed lines show the analytical results of linear MFT as given in Eqs. (76) and (83). In both cases, the CCF is computed according to Eqs. (57) and (60) based on the stress tensor. For illustrative purposes, we have chosen two representative temperatures: $x = 1$ (lower, red curves) and $x = 20$ (upper, blue curves).

However, for thick films ($x = (L/\xi)^{1/\nu} \rightarrow \infty$) the canonical scaling function diverges as

$$\frac{\Xi^{(c)}(x \gg 1)}{\Delta_0} \simeq 2\mathcal{M}^2\sqrt{x}. \quad (86)$$

This divergence is essentially a consequence of the OP constraint, as can be seen by inserting the constraint-induced chemical potential $\tilde{\mu}$ [Eq. (74)] into Eq. (71) in order to yield the canonical film pressure in Eq. (80). We demonstrate below [see, c.f., Eq. (92)] that the divergence stems from a *surface* contribution to the canonical film pressure.

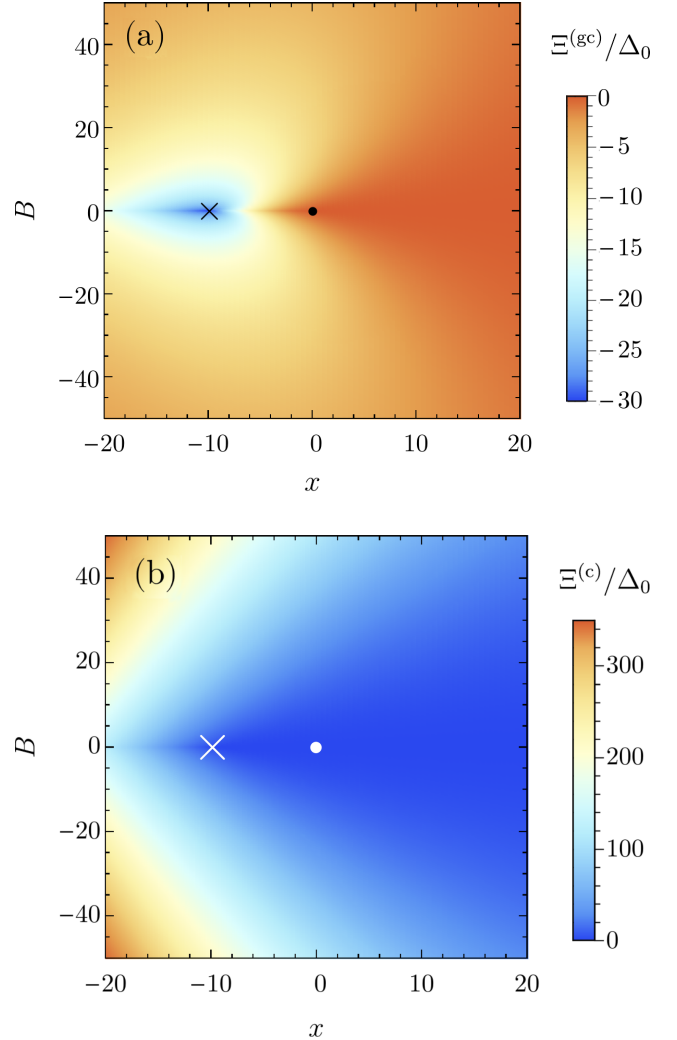


FIG. 10. The reduced scaling functions $\Xi^{(gc)}/\Delta_0$ (a) and $\Xi^{(c)}/\Delta_0$ (b) for the CCF in the grand canonical and canonical ensemble, respectively, obtained numerically from nonlinear MFT as function of the scaled bulk field B and the scaled temperature x . The cross (x) indicates the film critical point ($x = x_c^f = -\pi^2$, Eq. (34)), and the dot (•) the bulk critical point ($x = 0$). In (b), the cross and the dot are in white for better visibility. Note the different color codes.

B. Discussion of the CCF obtained within linear MFT and comparison with full, numerical results

The scaling functions $\Xi^{(c,gc)}$ of the CCF, as obtained from the stress tensor approach [Eqs. (57) and (60)] within nonlinear MFT, are illustrated in Fig. 9 (solid lines) as functions of the mass \mathcal{M} for two values of the scaled reduced temperature $x > 0$. The scaling functions are displayed in reduced form, i.e., divided by the mean-field amplitude Δ_0 [Eq. (15)], which is undetermined within MFT. Analytical results, obtained within linear MFT and given in Eqs. (76) and (83), are shown for comparison by the dashed lines. In Fig. 10, the numerically determined scaling functions, obtained within

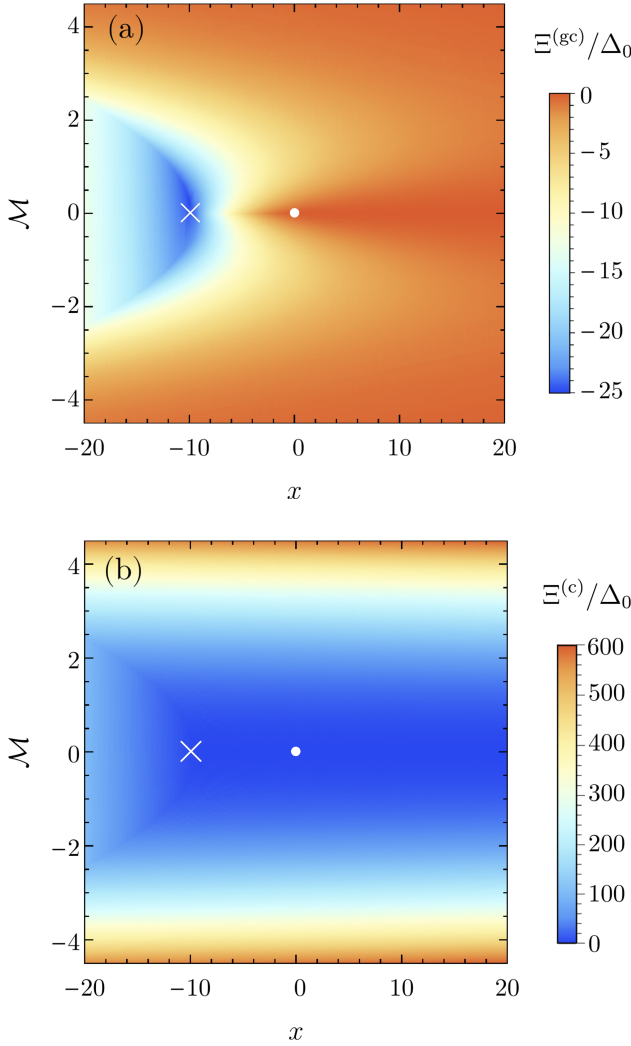


FIG. 11. The reduced scaling functions $\Xi^{(gc)}/\Delta_0$ (a) and $\Xi^{(c)}/\Delta_0$ (b) for the CCF in the grand canonical and canonical ensemble, respectively, obtained numerically from the nonlinear MFT as function of the scaled mass \mathcal{M} and scaled temperature x . The cross (\times) indicates the film critical point ($x = x_c^f = -\pi^2$, Eq. (34)), and the dot (\bullet) the bulk critical point ($x = 0$).

nonlinear MFT, are shown as functions of the scaled bulk field B and of x around the film and the bulk critical point (indicated by the cross and the dot, respectively).

As illustrated in Fig. 9, linear MFT generally provides an accurate approximation to full MFT for $\mathcal{M} \lesssim 1$ and $x \gtrsim 1$. Notably, within linear MFT and for all values of the reduced temperature $x > 0$ and the mass \mathcal{M} , the grand canonical CCF reported in Eq. (76) is attractive, i.e., $\Xi^{(gc)} < 0$, whereas the canonical CCF in Eq. (83) is repulsive, i.e., $\Xi^{(c)} > 0$ [58].

This character persists also within nonlinear MFT, as can be inferred from Fig. 10, where the behavior of the CCF scaling functions (determined via the stress tensor

approach) as function of the scaled bulk field B and the scaled temperature x is displayed. Figure 11 presents the same data as function of the scaled mass \mathcal{M} instead of B . In the grand canonical ensemble, generally the CCF is significant only around the film critical point (indicated by a cross in the plots). The canonical CCF, in contrast, shows the opposite behavior, growing with increasing distance from the critical region.

Notably, the difference in sign between the canonical and grand canonical CCF also occurs in the case of critical adsorption with symmetric surface fields (i.e., for $(++)$ boundary conditions) [15]. Furthermore, the behavior shown in Fig. 9(a) is consistent with MC results for Ising films in the grand canonical ensemble with a varying bulk field [30].

As stated above, the divergence of $\Xi^{(gc)}$ at the critical point is an artifact of linear MFT. Therefore the interval around \mathcal{M} , in which the scaling function of linear MFT provides an accurate approximation of the one of nonlinear MFT, becomes progressively narrower upon decreasing x . Furthermore, the exact $\Xi^{(gc)}$ is not quadratic in \mathcal{M} , but follows a rather nontrivial form as shown in Fig. 9(a) as well as in Figs. 10 and 11. In contrast, as demonstrated in Fig. 9(b), for sufficiently small $|\mathcal{M}|$, $\Xi^{(c)}$ obtained from nonlinear MFT is approximated well by linear MFT, even for $x \rightarrow 0$.

C. CCF deduced from the free energy

Here we determine the CCF explicitly from the residual finite-size free energy according to Eq. (55) and compare the result to the one obtained from a pressure difference [Eq. (57)].

1. Grand canonical CCF

Recalling the lowest order MFT solution in Eq. (24), we write the grand canonical free energy functional of the film given in Eq. (10) as

$$\begin{aligned} \mathcal{F}_f^{(gc)} &= \int_0^L dz \left[\frac{1}{2} (\partial_z \phi_0)^2 + \frac{1}{2} \tau \phi_0^2 - \mu \phi_0 \right] \\ &= \underbrace{-\frac{\mu^2 L}{2\tau}}_{\text{bulk}} + \underbrace{\frac{\mu^2}{\tau^{3/2}}}_{\text{surf.}} + \underbrace{\frac{\mu^2}{\tau^{3/2}} \left[\tanh\left(\frac{L\sqrt{\tau}}{2}\right) - 1 \right]}_{\text{residual}}. \end{aligned} \quad (87)$$

In the last line we have identified the various contributions according to their scaling with the film thickness L , keeping the bare parameters τ and μ fixed [see Eq. (56)]. Following Eq. (60), the grand canonical film pressure is

computed by differentiating the film free energy w.r.t. L while keeping the relevant control parameter, in this case $\mu = \tilde{\mu}$ [see Eq. (74)], fixed:

$$p_f^{(\text{gc})}(\tilde{\mu}) = -\partial_L \mathcal{F}_f^{(\text{gc})}|_{\tilde{\mu}} = \frac{\tau\varphi^2}{2} \frac{\tanh^2\left(\frac{L\sqrt{\tau}}{2}\right)}{\left(1 - \frac{2\tanh(L\sqrt{\tau}/2)}{L\sqrt{\tau}}\right)^2}. \quad (88)$$

As expected, Eq. (88) is identical to Eq. (80), which was obtained from the stress tensor. On the other hand, the CCF computed via Eq. (55),

$$\begin{aligned} -\partial_L \mathcal{F}_{\text{res}}^{(\text{gc})}|_{\mu} &= -\partial_L \left(\frac{\mu^2}{\tau^{3/2}} \tanh\left(\frac{L\sqrt{\tau}}{2}\right) \right) \\ &= -\frac{\mu^2}{\tau[1 + \cosh(L\sqrt{\tau})]} = \mathcal{K}_0^{(\text{gc})}, \end{aligned} \quad (89)$$

is identical to the expression in Eq. (73). Thus in the grand canonical ensemble, the CCF can be determined equivalently either via the stress tensor or via the residual free energy.

2. Canonical CCF

Inserting the constrained profile (Eq. (28)) into Eq. (9) yields the canonical free energy

$$\begin{aligned} \mathcal{F}_f^{(\text{c})} &= \int_0^L dz \left[\frac{1}{2}(\partial_z \tilde{\phi}_0)^2 + \frac{1}{2}\tau\tilde{\phi}_0^2 \right] \\ &= \frac{L\tau\varphi^2}{2} \left[\frac{1}{1 - \frac{2}{L\sqrt{\tau}} \tanh\left(\frac{L\sqrt{\tau}}{2}\right)} \right] \\ &= \underbrace{\frac{L\tau\varphi^2}{2}}_{\text{bulk}} + \underbrace{\frac{\sqrt{\tau}\varphi^2}{2}}_{\text{surf.}} + \underbrace{\sqrt{\tau}\varphi^2 \left[\frac{1}{\coth\left(\frac{L\sqrt{\tau}}{2}\right) - \frac{2}{L\sqrt{\tau}}} - 1 \right]}_{\text{residual}}. \end{aligned} \quad (90)$$

In the last equation, the various contributions have again been identified according to their scaling behavior as function of L , keeping the parameters τ and φ fixed, as it is appropriate for a finite-size scaling analysis in the canonical ensemble [see the discussion after Eq. (58)]. In order to obtain the film pressure via Eq. (60), the total mass Φ , which is the actual control parameter in the canonical ensemble, is kept fixed, yielding

$$p_f^{(\text{c})} = -\partial_L \mathcal{F}_f^{(\text{c})}|_{\Phi} = \frac{\tau\varphi^2}{2} \frac{\tanh^2\left(\frac{L\sqrt{\tau}}{2}\right)}{\left(1 - \frac{2\tanh(L\sqrt{\tau}/2)}{L\sqrt{\tau}}\right)^2}. \quad (91)$$

Since Eq. (91) and Eq. (80) are equal, herewith the equivalence of computing the film pressure via Eq. (60) or Eq. (63) is also established for the canonical ensemble. (Of course equality with the grand canonical film pressure holds, too.)

However, we note that the derivative (at fixed Φ) of the residual part of the free energy in Eq. (90) is not equal to the canonical CCF in Eq. (82) computed via the stress tensor:

$$\begin{aligned} -\partial_L \mathcal{F}_{\text{res}}^{(\text{c})}|_{\Phi} &= \left[\mathcal{K}_0^{(\text{c})} \text{ from Eq. (82)} \right] - \frac{2\varphi^2\sqrt{\tau}}{L} \\ &= \frac{\tau\varphi^2}{2} \left[\frac{\tanh^2\left(\frac{L\sqrt{\tau}}{2}\right)}{\left(1 - \frac{2\tanh(L\sqrt{\tau}/2)}{L\sqrt{\tau}}\right)^2} - 1 \right] - \frac{2\varphi^2\sqrt{\tau}}{L} \\ &= \tilde{\mathcal{K}}_0^{(\text{c})} = L^{-d} \tilde{\Xi}_0^{(\text{c})} \end{aligned} \quad (92)$$

with the reduced scaling function

$$\begin{aligned} \frac{\tilde{\Xi}_0^{(\text{c})}}{\Delta_0} &= \frac{\mathcal{M}^2 x}{2} \left[\frac{\tanh^2\left(\frac{\sqrt{x}}{2}\right)}{\left(1 - \frac{2}{\sqrt{x}} \tanh\left(\frac{\sqrt{x}}{2}\right)\right)^2} - 1 \right] \\ &\quad - 2\mathcal{M}^2\sqrt{x}. \end{aligned} \quad (93)$$

The canonical CCF $\tilde{\mathcal{K}}_0^{(\text{c})}$ is still repulsive, but instead of exhibiting the divergence $\propto \sqrt{x}$ in Eq. (86), it attains the finite limit

$$\frac{\tilde{\Xi}_0^{(\text{c})}(x \gg 1)}{\Delta_0} \simeq 6\mathcal{M}^2. \quad (94)$$

The term $-\frac{2\sqrt{\tau}\varphi^2}{L}$ in Eq. (92) would be absent if instead we would compute $-\partial_L \left(\mathcal{F}_{\text{res}}^{(\text{c})} + \mathcal{F}_{\text{surf}}^{(\text{c})} \right) |_{\Phi}$, where $\mathcal{F}_{\text{surf}}^{(\text{c})}$ denotes the surface contribution identified in Eq. (90). This indicates that the decomposition of $\mathcal{F}_f^{(\text{c})}$ according to the standard finite-size scaling arguments in Eq. (90) yields a surface contribution which is *not* independent of L , and thus contributes to the CCF in the canonical ensemble. This is a genuine consequence of the OP constraint $\Phi = \text{const}$. A similar observation has been made for the case of critical adsorption [15].

VII. MC SIMULATIONS OF THE ISING MODEL

In this section we determine the CCF via MC simulations of the Ising model in a thin film with Dirichlet boundary conditions in $d = 3$ spatial dimensions. We consider a simple cubic lattice of size $L_x \times L_y \times L_z$ with unit lattice spacing so that L_x , L_y , and L_z are dimensionless. We apply periodic boundary conditions along the x and y direction and Dirichlet boundary conditions

in the z direction. This means, that spins in the bottom layer have no bottom neighbor and spins in the top layer have no top neighbor. At each lattice site $i = (1 \leq x_i \leq L_x, 1 \leq y_i \leq L_y, 1 \leq z_i \leq L_z)$ a spin $s_i = \pm 1$ is located.

A. General simulation method

In the grand canonical ensemble and in the presence of a uniform bulk field μ , the Hamiltonian of the Ising model for a particular spin configuration ω is given by

$$\mathcal{H}^{(\text{gc})}(\omega) = -J \sum_{\langle ij \rangle} s_i s_j - \mu \sum_{\langle k \rangle} s_k. \quad (95)$$

The sum $\langle ij \rangle$ is taken over nearest neighbors on the lattice and the sum $\langle k \rangle$ runs over all spin sites. The energy and the bulk field μ are measured in units of the spin-spin interaction constant J so that they become dimensionless and $J = 1$. The grand canonical free energy of the system is

$$\beta \mathcal{F}^{(\text{gc})}(\beta, \mu) = -\ln \left[\sum_{\{\omega\}} \exp \left(-\beta \mathcal{H}^{(\text{gc})}(\omega) \right) \right], \quad (96)$$

where the sum is taken over all spin configurations $\{\omega\}$; $\beta = \frac{1}{k_B T}$ denotes the inverse thermal energy which in units of J is the dimensionless inverse temperature $\beta = 1/T$. The bulk critical point of the 3d Ising model occurs at the inverse temperature $\beta_c \simeq 0.22165455(3)$ [59]. We recall that, for a vanishing magnetic field $\mu = 0$, the correlation length is [see Eq. (5)] $\xi_t(t) = \xi_{\pm}^{(0)} t^{-\nu}$ whereas at the critical temperature the correlation length is $\xi_{\mu}(\mu) = \xi_{\mu}^{(0)} |\mu|^{-\nu/\Delta}$ with the value of the universal correlation length critical exponent $\nu = 0.63002(10)$ [60], the universal bulk magnetic field exponent $\Delta = 1.5637(14)$ [33], and with non-universal critical amplitudes $\xi_{\mu}^{(0)} = 0.278(2)$ [61], $\xi_-^{(0)} = 0.243(1)$, and $\xi_+^{(0)} = 0.501(2)$ [62].

The numerical simulation of the Ising model in the grand canonical ensemble has been performed by using a hybrid MC algorithm [63]: each MC step consists of a flip of a Wolf cluster followed by $L_x \times L_y \times L_z$ attempts to flip a randomly selected spin in accordance with the Metropolis rate. We perform simulations for a set of 32 points $0.17 \leq \beta_j \leq 0.28$ with a system of size $60 \times 60 \times 10$, corresponding to an aspect ratio of $L_z/L_{x(y)} \approx 0.167$. For each value of the inverse temperature β_j we have performed 32 simulations, using for each of them a different value μ_i of the bulk magnetic field with $0 \leq \mu_i \leq 0.15$. Subsequently, a histogram of the bulk magnetization $\tilde{\Phi} = \sum_{\langle k \rangle} s_k$ has been computed for each pair of parameters (β_j, μ_i) . The thermal average $\Phi = \langle \tilde{\Phi} \rangle$ has been taken over 10^6 MC steps, which

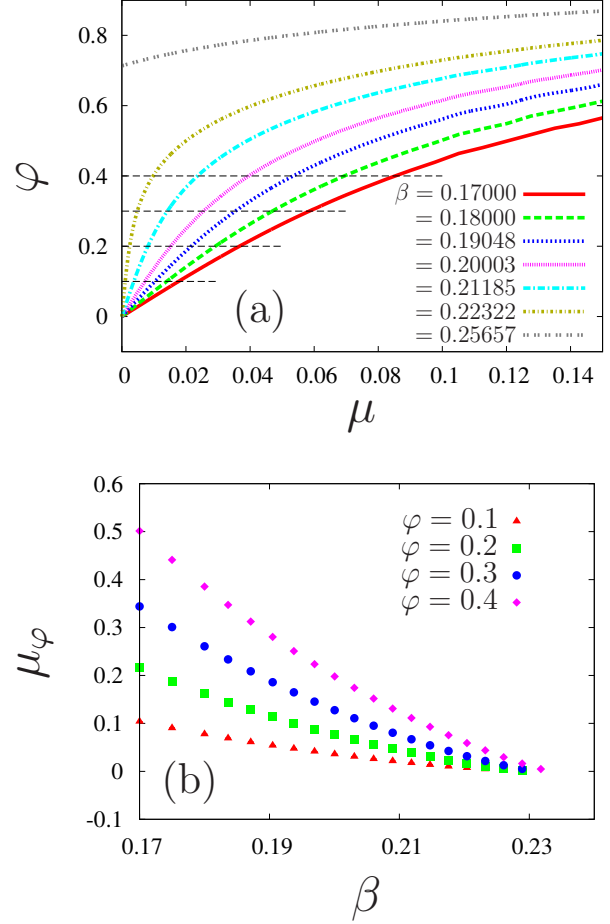


FIG. 12. MC simulation data (a) The magnetization φ per spin as a function of the bulk field μ for several values of the inverse temperature: $\beta = 0.17, 0.18, 0.19048, 0.20003, 0.21185, 0.22322, 0.25657$. (b) These bulk magnetic fields μ_φ as function of the inverse temperature β which render the values $\varphi = 0.1, 0.2, 0.3, 0.4$ of the mean magnetization in the grand canonical ensemble. The four values of φ considered in (b) are indicated in (a) by horizontal dotted lines. The value $\mu_\varphi = 0$ corresponds to $\varphi = 0$.

are split into 10 series in order to assess the numerical error. We have used the histogram reweighting technique [63] in order to compute the mean magnetization per spin $\varphi = \Phi/(L_x L_y L_z)$ [see Eq. (3)] as a continuous function of the bulk magnetic field μ . In Fig. 12(a), the magnetization φ per spin is shown as function of μ for several values of the inverse temperature β . This information has been used to compute that value μ_φ of the bulk magnetic field which renders the given mean magnetization φ per spin for a fixed value of β . In Fig. 12(b) we plot μ_φ as a function of β for several values of the magnetization φ per spin. These values of φ are also indicated in Fig. 12(a) by the horizontal dotted lines.

B. CCF in the grand canonical ensemble

1. Computation

The CCF $\mathcal{K}^{(gc)}(\beta, L_x, L_y, L)$ in the grand canonical ensemble can be computed on a lattice with cross-section $L_x \times L_y$ in terms of the finite difference of the free energies for two distinct slab thicknesses. Here, the actual thickness L considered in the calculation of the CCF is given by $L \equiv L_z - \frac{1}{2}$, because it is expressed via the difference of slabs of thickness L_z and $L_z - 1$:

$$\mathcal{K}^{(gc)}(\beta, \mu, L) \equiv - \frac{\beta \Delta \mathcal{F}^{(gc)}(\beta, \mu, L_x, L_y, L)}{L_x L_y} + \beta f_b^{(gc)}(\beta, \mu), \quad (97)$$

where the free energy difference is

$$\Delta \mathcal{F}^{(gc)}(\beta, \mu, L_x, L_y, L) = \mathcal{F}^{(gc)}(\beta, \mu, L_x, L_y, L + \frac{1}{2}) - \mathcal{F}^{(gc)}(\beta, \mu, L_x, L_y, L - \frac{1}{2}). \quad (98)$$

In the grand canonical ensemble with $\mu \neq 0$, we have computed the free energy difference $\Delta \mathcal{F}$ via the so-called coupling parameter approach. The bulk free energy density $f_b^{(gc)}$ has been computed for the same system but of size $60 \times 60 \times 120$, using the so-called energy integration technique. First, we have computed the bulk free energy at zero bulk field, upon integrating the energy over the inverse temperature. In the next step, for a given value of the inverse temperature, we have integrated the magnetization of the system over the bulk field, obtaining the bulk free energy for a given pair of variables (β_j, μ_i) (see Ref. [61] for further details). In d spatial dimensions the CCF can be expressed in terms of the corresponding scaling function $\Xi^{(gc)}$ as

$$\mathcal{K}^{(gc)}(\beta, \mu, L) = L_{\text{eff}}^{-d} \Xi^{(gc)}(L_{\text{eff}}/\xi_t, L_{\text{eff}}/\xi_\mu). \quad (99)$$

We have taken into account finite-size corrections via an effective slab thickness $L_{\text{eff}} \equiv L + \delta L$, with a correction $\delta L = 1.22(2)$ for Dirichlet boundary conditions [30].

2. Discussion

Fig. 13 shows the scaling function of the grand canonical CCF obtained from our MC simulations as function of the temperature scaling variable $t(L/\xi_+^{(0)})^{1/\nu} = x$ [Eq. (2b)] and of the bulk magnetic field μ . The behavior of $\Xi^{(gc)}$ obtained within MFT [see Fig. 10(a)] qualitatively agrees with our MC simulations. Consistently with previous studies [30], we find that the grand canonical CCF is attractive and reaches its greatest strength at vanishing bulk field $\mu = 0$ and at a slightly negative

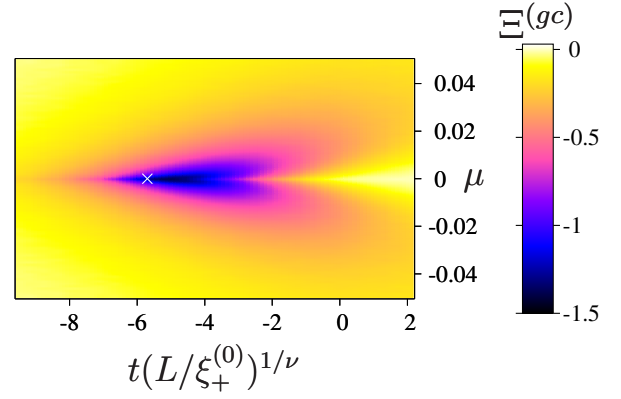


FIG. 13. MC results for the CCF scaling function $\Xi^{(gc)}$ for the grand canonical ensemble as function of the temperature scaling variable $t(L/\xi_+^{(0)})^{1/\nu}$ and the bulk magnetic field μ . The cross (x) indicates the film critical point of the Ising model [43].

reduced temperature $t < 0$. However, a more quantitative comparison is precluded due to appearance of the undetermined amplitude Δ_0 [Eq. (15)] arising within MFT. This deficiency can be overcome by including fluctuation effects within a renormalization group approach [44].

In Fig. 14(a) we illustrate the relationship between μ and the scaling variable $t(L/\xi_0^+)^{1/\nu}$ for various values of the mean magnetization φ . Figure 14(b) shows the CCF scaling function $\Xi^{(gc)}$ along lines of fixed magnetization φ as a function of $t(L/\xi_0^+)^{1/\nu}$. The CCF for $\varphi = 0$ — the data of which have been presented previously in Ref. [43] — is weak and attractive and an accurate, corresponding field theoretic description has been provided in Ref. [44]. The representation of the CCF in Figure 14(b) allows one to directly compare the grand canonical results with those in the canonical ensemble, to which we turn next.

C. CCF in the canonical ensemble

1. Computation

The Hamiltonian of the Ising model for the canonical ensemble is given by

$$\mathcal{H}^{(c)}(\omega) = -J \sum_{\langle ij \rangle} s_i s_j \quad (100)$$

and does not include the bulk magnetic field. The canonical free energy is obtained from the partition

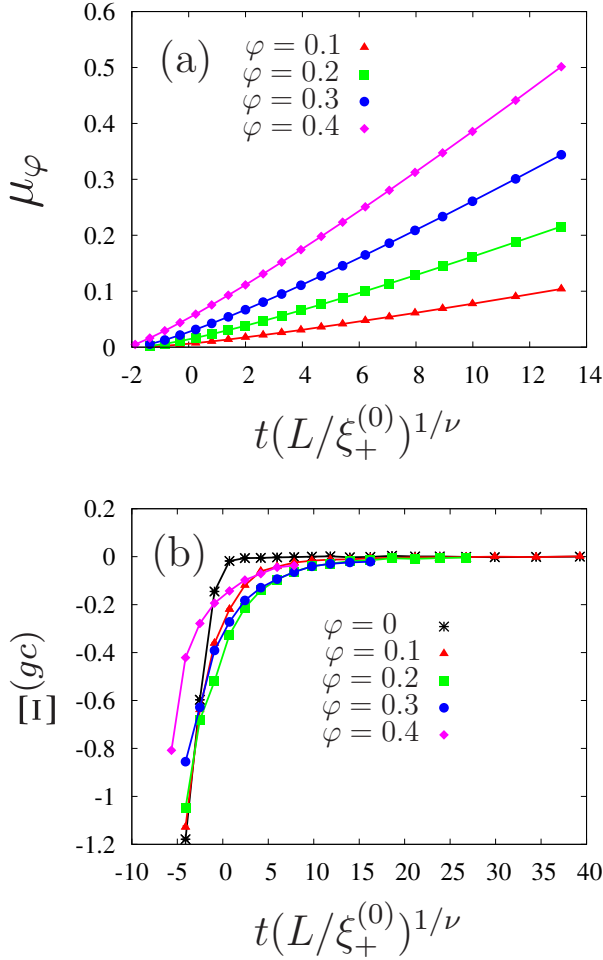


FIG. 14. MC results in the grand canonical ensemble. (a) Value μ_φ of the bulk magnetic field, at which the mean magnetization takes the values $\varphi = 0.1, 0.2, 0.3, 0.4$, as a function of the temperature scaling variable $t(L/\xi_+^{(0)})^{1/\nu}$. In the considered temperature region, $\varphi = 0$ corresponds to $\mu_\varphi = 0$. (b) The scaling function $\Xi^{(gc)}$ of the grand canonical CCF as a function of the temperature scaling variable $t(L/\xi_+^{(0)})^{1/\nu}$, computed along the lines $(t(L/\xi_+^{(0)})^{1/\nu}, \mu_\varphi)$ in (a) for the mean magnetizations $\varphi = 0, 0.1, 0.2, 0.3, 0.4$.

function as

$$\beta \mathcal{F}^{(c)}(\beta, m) = -\ln \left[\sum_{\{\omega\}} \delta(Nm, \sum_{\langle k \rangle} s_k(\omega)) \times \exp \left(-\beta \mathcal{H}^{(c)}(\omega) \right) \right], \quad (101)$$

where the Kronecker delta function selects only terms corresponding to spin configurations ω with fixed, prescribed magnetization $\Phi = \varphi N = \sum_{\langle k \rangle} s_k(\omega)$. Here,

$N = L_x \times L_y \times L_z$ denotes the total number of spins in the system. A configuration of N spins with a magnetization φ per spin contains $N_+ = \frac{1+\varphi}{2}N$ up spins and $N_- = \frac{1-\varphi}{2}N$ down spins. At infinite temperature

$\beta = 0$, the free energy of the canonical ensemble can be expressed as

$$\beta \mathcal{F}^{(c)}(\beta, \varphi, N)|_{\beta=0} = -\ln \left(\frac{N!}{N_+! N_-!} \right). \quad (102)$$

Using Stirling's formula $n! \simeq \sqrt{2\pi n} n^{n+\frac{1}{2}} \exp(-n)$, one obtains for the bulk free energy per spin $\beta f_b^{(c)} = \frac{1}{N} \beta \mathcal{F}_b^{(c)}(\beta, m, N)$ in the limit of high temperatures ($\beta = 0$) and large system sizes N

$$\beta f_b^{(c)}(\beta, \varphi)|_{\beta=0} = \frac{1+\varphi}{2} \ln \left(\frac{1+\varphi}{2} \right) + \frac{1-\varphi}{2} \ln \left(\frac{1-\varphi}{2} \right) + \frac{1}{2N} \ln \left(\frac{\pi}{2} (1+\varphi)(1-\varphi) \right). \quad (103)$$

We note that in principle the canonical free energy density in Eq. (103) differs from the grand canonical free energy density, which at infinite temperature is $\beta f_b^{(gc)}(\beta)|_{\beta=0} = -\ln(2)$. Only for zero magnetization $\varphi = 0$ these two quantities coincide, *i.e.*, $\beta f_b^{(c)}(\beta, \varphi = 0)|_{\beta=0} = -\ln(2)$.

For the canonical ensemble we have computed the free energy for a system with cross-section $L_x \times L_y$ and thickness L_z ($N = L_x \times L_y \times L_z$) via integration of the mean energy E per spin over the inverse temperature β :

$$\beta \mathcal{F}^{(c)}(\beta, \varphi, L_z) = -\ln \left(\frac{N!}{N_+! N_-!} \right) + \int_0^\beta E^{(c)}(\beta', \varphi, L_z) d\beta'. \quad (104)$$

The internal energy $E^{(c)}$ of the canonical system with a fixed magnetization φ per spin has been computed based on Kawasaki dynamics [64]. Typically we have used 5×10^7 MC steps for thermalization (one MC step consists of N attempts of pair Kawasaki exchanges), followed by 10^8 MC steps for computing the thermal average. Using Eq. (104) we have determined the free energy difference $\Delta \mathcal{F}^{(c)}(\beta, \varphi, L_x, L_y, L) = \mathcal{F}^{(c)}(\beta, \varphi, L_x, L_y, L + \frac{1}{2}) - \mathcal{F}^{(c)}(\beta, \varphi, L_x, L_y, L - \frac{1}{2})$. Without knowledge of the bulk free energy density $f_b^{(c)}$ we can apply the method introduced in Ref. [65], which provides the following difference:

$$g_C(\beta, \varphi, L) = \beta [\Delta \mathcal{F}^{(c)}(\beta, \varphi, L_x, L_y, L) - \Delta \mathcal{F}^{(c)}(\beta, \varphi, L_x, L_y, 2L)]. \quad (105)$$

Considering therein the second term as an estimate of a difference of the bulk free energy, we approximate the canonical CCF as $\mathcal{K}^{(c)}(\beta, \varphi, L) \approx g_C(\beta, \varphi, L)$. Accordingly, the associated scaling function follows, analogously to Eq. (99), as

$$\Xi^{(c)}(L_{\text{eff}}/\xi_t, \varphi) \simeq L_{\text{eff}}^d g_C(\beta, \varphi, L). \quad (106)$$

In order to numerically determine $\Xi^{(c)}$ via Eq. (106), we have performed MC simulations for a system of size $L_x = L_y = 60$, $L_z = 10$, and we have assumed an effective thickness $L_{\text{eff}} = L + 1.22$ as in the grand canonical case.

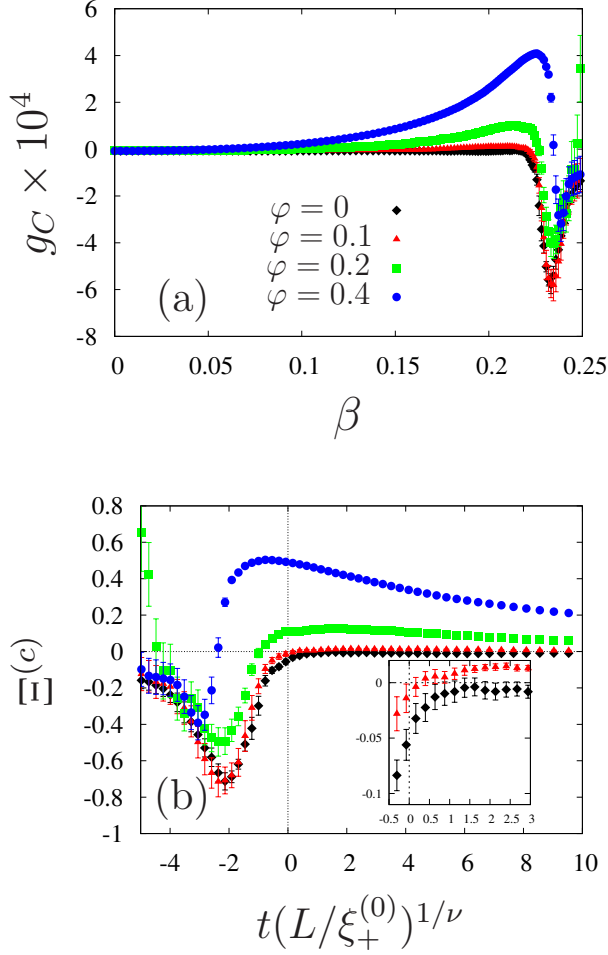


FIG. 15. MC results in the canonical ensemble. (a) Auxiliary function g_C [Eq. (105)] as a function of the inverse temperature β for $\varphi = 0, 0.1, 0.2, 0.4$. (b) Scaling function $\Xi^{(c)}$ of the canonical CCF [Eq. (106)] as function of the scaled temperature $t(L/\xi_+^{(0)})^{1/\nu}$ for three mean magnetizations $\varphi = 0, 0.1, 0.2, 0.4$.

2. Discussion

In Fig. 15(a) the auxiliary function g_C [Eq.(105)] is plotted as a function of β for $\varphi = 0, 0.1, 0.2, 0.4$. Figure 15(b) shows the scaling function $\Xi^{(c)}$ of the canonical CCF obtained via Eq. (106) as a function of the scaled temperature $t(L/\xi_+^{(0)})^{1/\nu}$ for various mean magnetizations $\varphi > 0$. In contrast to the grand canonical ensemble [see Fig. 14(b)], the canonical CCF obtained from MC simulations is repulsive (*i.e.*, $\Xi^{(c)} > 0$) for $\varphi \gtrsim 0.1$ and for supercritical temperatures $x > 0$. The repulsive character and the fact, that the strength of the canonical CCF increases with growing $|\varphi|$, are captured correctly by MFT [see Fig. 11(b)]. Note, however, that, within MFT, the canonical CCF is repulsive across the whole parameter range considered here, except at $\varphi = 0$,

where $\Xi^{(c)} = 0$. The discrepancy between MC results and MFT concerning the sign of the CCF for $t > 0$ and as $\varphi \rightarrow 0$ is due to the effect of critical fluctuations, which render a weak but attractive canonical CCF, in agreement with the predictions in Ref. [16], [66]. A detailed analysis of the CCF for subcritical bulk temperatures ($t < 0$), for which, in contrast to the predictions of MFT, a pronounced minimum appears, is left for future studies.

VIII. SUMMARY

We have studied ensemble differences of the OP profile and of the CCF, arising in a critical fluid film of thickness L within the so-called ordinary surface universality class at both walls. In the grand canonical ensemble, the film can exchange material with its environment at a common chemical potential μ . In the canonical ensemble, instead, particle exchange is prohibited and the film and the environment are taken to have the same mean OP density φ . The system is analyzed within mean field theory, *i.e.*, neglecting thermal fluctuations. In this limit, the CCF stems solely from the action of an external bulk field (such as the chemical potential μ) or, correspondingly, from a nonzero total mass $\Phi = \int_0^L dz \phi(z) = L\varphi$. We generally assume translational invariance in the lateral directions of the film and, accordingly, we consider all extensive quantities as defined *per transverse area* A [compare Eq. (1)].

Our findings can be summarized as follows:

1. We have solved the Euler-Lagrange equations for the OP profile in the film via three complementary approaches: (i) a perturbative solution in terms of orders of the nonlinear term in the supercritical regime ($T \geq T_c^b$), (ii) an exact solution below the film critical point, *i.e.*, for $T \leq T_c^f < T_c^b$ and at vanishing external bulk field ($\mu = 0$), and (iii) a numerical solution for arbitrary values of the temperature and of the bulk field. For small values of the scaled mass $|\mathcal{M}|$ or, respectively, the scaled bulk field $|B|$, the perturbative solution generally provides an accurate approximation of the exact mean field solution [see Figs. 2, 3, and 4].
2. The scaling behavior of the scaled mass $\mathcal{M}(x, B)$ as function of the scaled temperature x and the scaled bulk field B has been analyzed based on the full MFT in various asymptotic limits [see Figs. 5, 6, and 7]. In the case of a vanishing bulk field ($B = 0$), the exact expression for $\mathcal{M}(x)$ has been determined in Eq. (40). For general B , we have explicitly demonstrated that Widom's scaling hypothesis applies for the system studied here [see Fig. 8].

3. We have analyzed the CCF within linear and non-linear MFT in the canonical and the grand canonical ensembles. For $\mathcal{M} = 0$ and $x > 0$, both the canonical and the grand canonical CCF vanish within MFT. For $\mathcal{M} \neq 0$ and within the studied parameter region around the film and bulk critical points [see Figs. 9, 10, and 11], the grand canonical CCF is *attractive* (consistent with Ref. [30]), while the canonical CCF is *repulsive*.
4. The canonical CCF depends on whether it is defined as the difference between the film and the bulk pressure [Eq. (57)] or as a derivative of the residual finite-size free energy [Eq. (55)]. The difference between the two approaches stems from a surface-like pressure contribution [see Eq. (92)], which is a direct consequence of the global OP constraint in the canonical ensemble.
5. The grand canonical CCF generally vanishes in the limit $x \rightarrow \infty$, as expected. In contrast, the canonical CCF defined as a pressure difference [Eq. (57)] diverges $\propto x$ in this limit [see Eq. (86)], while the canonical CCF extracted from the residual finite-size free energy [Eq. (55)] approaches a nonzero constant [see Eq. (94)]. These unexpected limiting behaviors are again induced by the OP constraint acting in the canonical ensemble.
6. We have studied the influence of fluctuations onto the CCF via MC simulations of the $d = 3$ dimensional Ising model. The predictions of MFT are qualitatively recovered by the simulations for sufficiently large values of the magnetization φ , while fluctuations dominate for $|\varphi| \ll 1$. In agreement

with MFT, we find that the grand canonical CCF is attractive within the studied parameter ranges of x and φ [see Figs. 13 and 14(b)]. At supercritical temperatures ($t > 0$), the canonical CCF is repulsive for large mean magnetizations $|\varphi| \gg 1$ and (weakly) attractive for small mean magnetizations [see Fig. 15(b)]. Below the bulk critical point, a pronounced minimum of the canonical CCF is observed. Note that a quantitative comparison between MFT and MC simulations is precluded by the undetermined amplitude Δ_0 [Eq. (15)] appearing in the mean-field scaling functions.

We remark that certain characteristic features of the canonical CCF found here, such as its repulsive character, its dependence on the precise definition [i.e., Eq. (55) vs. Eq. (57)], and its nontrivial decay behavior for thick films ($x \gg 1$), appear analogously also in the case of critical films confined by walls with parallel surface fields [15].

Critical fluids typically show strong adsorption at the container walls [7–9]. In order to experimentally study the results obtained here, it would thus be necessary to suitably modify the walls in order to obtain effective Dirichlet boundary conditions for the OP. As has been shown previously, this can be achieved by endowing the surfaces with narrow chemical stripes of antagonistic character [10–14]. Together with Refs. [15, 16], the present study provides further evidence that the CCF crucially depends on the thermodynamic ensemble under consideration and, in particular, on the presence of OP constraints.

Appendix A: Solution of Eq. (18) at $\mathcal{O}(\epsilon^2)$

In terms of the formal expansion of the OP m and of the bulk field B (see Eq. (20)), at $\mathcal{O}(\epsilon^2)$ the ELE [Eq. (18)] reads

$$m_2'' = xm_2 + 3m_0^2m_1 - B_2. \quad (\text{A1})$$

While the full solution of Eq. (A1) is omitted here, we report the expression for the constraint-induced field $B_2 = \tilde{B}_2$:

$$\begin{aligned} \tilde{B}_2 = & \frac{\mathcal{M}^5 x^{3/2}}{15360 \left(\sqrt{x} \cosh\left(\frac{\sqrt{x}}{2}\right) - 2 \sinh\left(\frac{\sqrt{x}}{2}\right) \right)^7} \\ & \times \left[-2025\sqrt{x}(8x + 121) \sinh\left(\frac{\sqrt{x}}{2}\right) - 216\sqrt{x}(75x + 1256) \sinh\left(\frac{3\sqrt{x}}{2}\right) \right. \\ & - 24\sqrt{x}(135x + 2518) \sinh\left(\frac{5\sqrt{x}}{2}\right) - 681\sqrt{x} \sinh\left(\frac{7\sqrt{x}}{2}\right) + 50(4410x - 3659) \cosh\left(\frac{\sqrt{x}}{2}\right) \\ & \left. + 648(160x + 171) \cosh\left(\frac{3\sqrt{x}}{2}\right) + 40(432x + 1685) \cosh\left(\frac{5\sqrt{x}}{2}\right) + 4742 \cosh\left(\frac{7\sqrt{x}}{2}\right) \right], \quad (\text{A2}) \end{aligned}$$

which has the following asymptotic scaling behavior:

$$\tilde{B}_2 \rightarrow \begin{cases} -\frac{8343}{175175}\mathcal{M}^5, & x \rightarrow 0, \\ \sim -\frac{227}{80}\mathcal{M}^5 x^{-3/2} \rightarrow 0, & x \rightarrow \infty. \end{cases} \quad (\text{A3})$$

The constrained profile scales as

$$\tilde{m}_2(\zeta) \rightarrow \begin{cases} p^{(14)}(\zeta - 1/2), & x \rightarrow 0, \\ 0, & x \rightarrow \infty, \end{cases} \quad (\text{A4})$$

where $p^{(14)}$ represents the 14th-order polynomial

$$p^{(14)}(y) = -\frac{81\mathcal{M}^5}{1435033600} \left[40550400y^{14} - 106229760y^{12} + 134278144y^{10} - 91703040y^8 + 35939904y^6 - 8408400y^4 + 959492y^2 - 25365 \right]. \quad (\text{A5})$$

-
- [1] M. E. Fisher and P. G. de Gennes, “Wall Phenomena in a Critical Binary Mixture,” *C. R. Acad. Sci. Paris B* **287**, 207 (1978).
 - [2] M. Krech, *The Casimir effect in critical systems* (World Scientific, Singapore, 1994).
 - [3] H. W. Diehl, “Field-theoretical Approach to Critical Behavior at Surfaces,” in *Phase Transitions and Critical Phenomena*, Vol. 10, edited by C. Domb and J. L. Lebowitz (Academic, London, 1986) p. 76.
 - [4] H. W. Diehl, “The Theory of Boundary Critical Phenomena,” *Int. J. Mod. Phys. B* **11**, 3503–3523 (1997).
 - [5] J. G. Brankov, D. M. Dantchev, and N. S. Tonchev, *The Theory of Critical Phenomena in Finite-Size Systems* (World Scientific, Singapore, 2000).
 - [6] Michael E. Fisher and Hisao Nakanishi, “Scaling theory for the criticality of fluids between plates,” *J. Chem. Phys.* **75**, 5857–5863 (1981).
 - [7] Andrea J. Liu and Michael E. Fisher, “Universal critical adsorption profile from optical experiments,” *Phys. Rev. A* **40**, 7202–7221 (1989).
 - [8] G. Flöter and S. Dietrich, “Universal amplitudes and profiles for critical adsorption,” *Z. Phys. B* **97**, 213–232 (1995).
 - [9] A. Gambassi, A. Maciolek, C. Hertlein, U. Nellen, L. Helden, C. Bechinger, and S. Dietrich, “Critical Casimir effect in classical binary liquid mixtures,” *Phys. Rev. E* **80**, 061143 (2009).
 - [10] U. Nellen, L. Helden, and C. Bechinger, “Tunability of critical Casimir interactions by boundary conditions,” *EPL* **88**, 26001 (2009).
 - [11] Monika Sprenger, Frank Schlesener, and Siegfried Dietrich, “Forces between chemically structured substrates mediated by critical fluids,” *J. Chem. Phys.* **124**, 134703 (2006).
 - [12] M. Tröndle, S. Kondrat, A. Gambassi, L. Harnau, and S. Dietrich, “Normal and lateral critical Casimir forces between colloids and patterned substrates,” *EPL* **88**, 40004 (2009).
 - [13] M. Tröndle, S. Kondrat, A. Gambassi, L. Harnau, and S. Dietrich, “Critical Casimir effect for colloids close to chemically patterned substrates,” *J. Chem. Phys.* **133**, 074702 (2010).
 - [14] Andrea Gambassi and S. Dietrich, “Critical Casimir forces steered by patterned substrates,” *Soft Matter* **7**, 1247–1253 (2011).
 - [15] Markus Gross, Oleg Vasilyev, Andrea Gambassi, and S. Dietrich, “Critical adsorption and critical Casimir forces in the canonical ensemble,” *Phys. Rev. E* **94**, 022103 (2016).
 - [16] Markus Gross, Andrea Gambassi, and S. Dietrich, “Statistical field theory with constraints: Application to critical Casimir forces in the canonical ensemble,” *Phys. Rev. E* **96**, 022135 (2017).
 - [17] E. Eisenriegler and R. Tomaschitz, “Helmholtz free energy of finite spin systems near criticality,” *Phys. Rev. B* **35**, 4876–4887 (1987).
 - [18] J. G. Brankov and D. M. Danchev, “A probabilistic view on finite-size scaling in infinitely coordinated spherical models,” *Physica A* **158**, 842–863 (1989).
 - [19] H. W. J. Blöte, J. R. Heringa, and M. M. Tsypin, “Three-dimensional Ising model in the fixed-magnetization ensemble: A Monte Carlo study,” *Phys. Rev. E* **62**, 77–82 (2000).
 - [20] S. Caracciolo, A. Gambassi, M. Gubinelli, and A. Pelissetto, “Finite-size correlation length and violations of finite-size scaling,” *Eur. Phys. J. B* **20**, 255–265 (2001).
 - [21] M. Pleimling and A. Hüller, “Crossing the Coexistence Line at Constant Magnetization,” *J. Stat. Phys.* **104**, 971–989 (2001).
 - [22] M. Krech and S. Dietrich, “Finite-size scaling for critical films,” *Phys. Rev. Lett.* **66**, 345–348 (1991).
 - [23] M. Krech and S. Dietrich, “Free energy and specific heat of critical films and surfaces,” *Phys. Rev. A* **46**, 1886–1921 (1992).
 - [24] M. Krech and S. Dietrich, “Specific heat of critical films, the Casimir force, and wetting films near critical end points,” *Phys. Rev. A* **46**, 1922–1941 (1992).
 - [25] Felix M. Schmidt and H. W. Diehl, “Crossover from Attractive to Repulsive Casimir Forces and Vice Versa,” *Phys. Rev. Lett.* **101**, 100601 (2008).

- [26] Martin Hasenbusch, “Thermodynamic Casimir force: A Monte Carlo study of the crossover between the ordinary and the normal surface universality class,” *Phys. Rev. B* **83**, 134425 (2011).
- [27] H. W. Diehl and Felix M. Schmidt, “The critical Casimir effect in films for generic non-symmetry-breaking boundary conditions,” *New. J. Phys.* **13**, 123025 (2011).
- [28] T. F. Mohry, A. Maciolek, and S. Dietrich, “Crossover of critical Casimir forces between different surface universality classes,” *Phys. Rev. E* **81**, 061117 (2010).
- [29] O. Vasilyev, A. Maciolek, and S. Dietrich, “Critical Casimir forces for Ising films with variable boundary fields,” *Phys. Rev. E* **84**, 041605 (2011).
- [30] O. A. Vasilyev and S. Dietrich, “Critical Casimir forces for films with bulk ordering fields,” *EPL* **104**, 60002 (2013).
- [31] Valdimir Privman and Michael E. Fisher, “Universal critical amplitudes in finite-size scaling,” *Phys. Rev. B* **30**, 322–327 (1984).
- [32] V. Privman, “Finite-Size Scaling Theory,” in *Finite Size Scaling and Numerical Simulation of Statistical Systems*, edited by V. Privman (World Scientific, Singapore, 1990) p. 1.
- [33] Andrea Pelissetto and Ettore Vicari, “Critical phenomena and renormalization-group theory,” *Phys. Rep.* **368**, 549–727 (2002).
- [34] Kurt Binder, “Critical Behavior at Surfaces,” in *Phase Transitions and Critical Phenomena*, Vol. 8, edited by C. Domb and J. L. Lebowitz (Academic, London, 1983) p. 1.
- [35] Daniel Dantchev, Michael Krech, and S. Dietrich, “Universality of the thermodynamic Casimir effect,” *Phys. Rev. E* **67**, 066120 (2003).
- [36] X. S. Chen and V. Dohm, “Nonuniversal finite-size scaling in anisotropic systems,” *Phys. Rev. E* **70**, 056136 (2004).
- [37] Daniel Dantchev, Frank Schlesener, and S. Dietrich, “Interplay of critical Casimir and dispersion forces,” *Phys. Rev. E* **76**, 011121 (2007).
- [38] Volker Dohm, “Diversity of critical behavior within a universality class,” *Phys. Rev. E* **77**, 061128 (2008).
- [39] H. W. Diehl and H. Chamati, “Dynamic critical behavior of model A in films: Zero-mode boundary conditions and expansion near four dimensions,” *Phys. Rev. B* **79**, 104301 (2009).
- [40] W. Selke and L. N. Shchur, “Critical Binder cumulant in a two-dimensional anisotropic Ising model with competing interactions,” *Phys. Rev. E* **80**, 042104 (2009).
- [41] Volker Dohm, “Crossover from low-temperature to high-temperature fluctuations: Universal and nonuniversal Casimir forces of isotropic and anisotropic systems,” *Phys. Rev. E* **97**, 062128 (2018).
- [42] A. Gambassi and S. Dietrich, “Critical Dynamics in Thin Films,” *J. Stat. Phys.* **123**, 929 (2006).
- [43] O. Vasilyev, A. Gambassi, A. Maciolek, and S. Dietrich, “Universal scaling functions of critical Casimir forces obtained by Monte Carlo simulations,” *Phys. Rev. E* **79**, 041142 (2009).
- [44] Volker Dohm, “Pronounced minimum of the thermodynamic Casimir forces of O(n) symmetric film systems: Analytic theory,” *Phys. Rev. E* **90**, 030101 (2014).
- [45] I. S. Gradshteyn and I. M. Ryzhik, *Table of Integrals, Series, and Products* (Academic, London, 2014).
- [46] Frank W. J. Olver, Daniel W. Lozier, Ronald F. Boisvert, and Charles W. Clark, *NIST Handbook of Mathematical Functions*, 1st ed. (Cambridge University Press, 2010).
- [47] Ronald D. Ruth, “A canonical integration technique,” *IEEE Trans. Nucl. Sci.* **30**, 2669–2671 (1983).
- [48] Ernst Hairer, Christian Lubich, and Gerhard Wanner, *Geometric Numerical Integration: Structure-Preserving Algorithms for Ordinary Differential Equations*, 2nd ed. (Springer, Heidelberg, 2010).
- [49] Hisao Nakanishi and Michael E. Fisher, “Critical point shifts in films,” *J. Chem. Phys.* **78**, 3279–3293 (1983).
- [50] B. Widom, “Equation of State in the Neighborhood of the Critical Point,” *J. Chem. Phys.* **43**, 3898–3905 (1965).
- [51] H. E. Stanley, *Introduction to Phase Transitions and Critical Phenomena*, revised ed. (Oxford University Press USA, New York, 1971).
- [52] L. P. Kadanoff, W. Götzke, D. Hamblen, R. Hecht, E. A. S. Lewis, V. V. Palciauskas, M. Rayl, J. Swift, D. Aspnes, and J. Kane, “Static Phenomena Near Critical Points: Theory and Experiment,” *Rev. Mod. Phys.* **39**, 395–431 (1967).
- [53] V. Dohm, “Critical Casimir force in slab geometry with finite aspect ratio: Analytic calculation above and below T_c ,” *EPL* **86**, 20001 (2009).
- [54] H. W. Diehl, Daniel Grüneberg, Martin Hasenbusch, Alfred Hucht, Sergei B. Rutkevich, and Felix M. Schmidt, “Large- n approach to thermodynamic Casimir effects in slabs with free surfaces,” *Phys. Rev. E* **89**, 062123 (2014).
- [55] Boris Kastening and Volker Dohm, “Finite-size effects in film geometry with nonperiodic boundary conditions: Gaussian model and renormalization-group theory at fixed dimension,” *Phys. Rev. E* **81**, 061106 (2010).
- [56] Daniel Dantchev, H. W. Diehl, and Daniel Grüneberg, “Excess free energy and Casimir forces in systems with long-range interactions of van der Waals type: General considerations and exact spherical-model results,” *Phys. Rev. E* **73**, 016131 (2006).
- [57] In the canonical ensemble the actual thermodynamic control parameter is the total mass Φ . However, as discussed in detail in Ref. [15], for the purpose of determining the finite-size limit in Eq. (58), instead the mass density φ should be kept fixed.
- [58] In order to prove that $\Xi^{(c)} > 0$, set $y = \sqrt{x}/2$ in Eq. (83) and first note that $1 - \tanh(y)/y > 0$ for $y > 0$. Accordingly, $\Xi^{(c)} > 0$ [Eq. (83)] is equivalent to $\tanh(y) > y/(1+y)$. The validity of the latter inequality can be readily shown by considering the derivatives and expressing the hyperbolic functions in terms of exponentials.
- [59] Y. Deng and H. W. J. Blöte, “Simultaneous analysis of several models in the three-dimensional Ising universality class,” *Phys. Rev. E* **68**, 036125 (2003).
- [60] M. Hasenbusch, “Finite size scaling study of lattice models in the three-dimensional Ising universality class,” *Phys. Rev. B* **82**, 174433 (2010).
- [61] O. Vasilyev, “Monte Carlo Simulation of Critical Casimir Forces,” in *Order, Disorder and Criticality: Advanced Problems of Phase Transition Theory*, Vol. 4 (World Scientific, Singapore, 2015) p. 55.
- [62] C. Ruge, P. Zhu, and F. Wagner, “Correlation function in Ising models,” *Physica A* **209**, 431–443 (1994).

- [63] David P. Landau and Kurt Binder, *A Guide to Monte Carlo Simulations in Statistical Physics*, 3rd ed. (Cambridge University Press, 2009).
- [64] Kyozi Kawasaki, “Diffusion Constants near the Critical Point for Time-Dependent Ising Models. I,” *Phys. Rev.* **145**, 224–230 (1966).
- [65] O. Vasilyev, A. Gambassi, A. Maciolek, and S. Dietrich, “Monte Carlo simulation results for critical Casimir forces,” *EPL* **80**, 60009 (2007).
- [66] The high-temperature limit of $\Xi^{(c)}$ for $\varphi = 0$ obtained from MC simulations differs from the theoretical expectation $\Xi^{(c)} \simeq -\varrho^{d-1}/2$ (where $\varrho = L_z/L_{x,y}$ is the aspect ratio) mainly due to the approximations involved in Eq. (105).